Hydrodynamic Simulation of Oil Sand Multiphase Flow in At Face Slurry System

by

Enzu Zheng

A thesis submitted in partial fulfillment of the requirements for the degree of

Master of Science

in

Mining Engineering

Department of Civil and Environmental Engineering

University of Alberta

Abstract

Hydraulic transportation efficiency and production cost optimization are required in the surface extraction of Athabasca oil sand deposits. Currently, stationary pipelines are used for slurry transportation in many mines. In order to reduce the dependence on haulage truck for long haulage distances, there is a desire to extend the hydraulic transport system to production faces in oil sands mines using mobile At Face Slurry System (AFSS). The AFSS consists of pipelines connected together with flexible joints and would be capable to create slurrified minerals from the mining faces to be transported to the processing plant. Slurry transportation based on mobile pipelines has been shown to be more effective than the shovel-truck haulage system. This flexible arrangement introduces a unique set of hydraulic transport problems. Rigorous modeling and experimentation of oil sand slurry multiphase flow in this mobile system are required to understand its technical viability and effectiveness. The thesis focuses to develop the mathematic models governing the friction loss of oil sand slurry associated with the AFSS. Computational Fluid Dynamics (CFD) simulation of slurry flow using the academic package Ansys-Fluent 14.5 is conducted. A flexible arrangement of pipe loops imitating the AFSS are set up in the laboratory. Experimental and modelling results are compared to test the accuracy of CFD modelling to predict friction loss in the flexible pipeline system. Results indicate that Granular-Eulerian Multiphase model is reasonably effective in predicting the pressure drop of the at face slurry loop (with a percentage error in the range $\pm$10%) at all the solid concentrations under different configurations. For oil sand slurry with specific gravity 1.44, solid volume fraction 0.27 and velocity 4 m/s, the simulated pressure gradient associated with the AFSS of diameter 0.762m is 220Pa/m, compared with the 158Pa/m for the existing stationary system at Syncrude under the same conditions.

Acknowledgements

I would like to extend my deep gratitude to Prof. Jozef Szymanski, my supervisor, who has provided me with this research opportunity and given me patient guidance and great support. I would also like to thank Prof. Tim Joseph for his unending support and guidance on my graduate study.

I am grateful to have worked with every member of AEGIS research group who give me encouragement, assistance, and suggestions during the course of my research.

I acknowledge the University of Alberta and the Faculty of Civil and Environmental Engineering which provide me with the research assistantship as well as the financial support.

Finally thanks to my families who give me love and support.

Contents

List of Figures

List of Tables

1 Introduction

1.1 Background of the Problem

Large-capacity shovels and dump trucks are increasingly utilized for excavation, loading and hauling in the operation of surface mining. Production cost and efficiency optimization are demanded during the Athabasca oil sands mining process in order to secure North America's energy supply. However, increasing haulage distances, rugged terrain and constrained mine environment will reduce the effectiveness of the shovel-truck haulage system (Frimpong, 2003). In such conditions, tires are susceptible to failures with the tire heat index and the ton/km/h limit for truck haulage exceeded, simultaneously creating extreme tire wear and high maintenance costs. Besides production cost and equipment effectiveness, a mining environment also requires efficient waste materials recycling and distribution. Waste materials need to be recycled from the processing plant to a new destination like tailings dam, or to the mined out areas as a backfill. With such configuration and location characteristics, the mining environment requires flexible pipelines for access and efficient recycling process.

Slurry transportation is an economic and viable alternative in oil sands operations. Alberta, as the primary supply and service hub for Canada's crude oil and oil sands industries, it might represent the world's most intensive slurry pipeline technology application. Three operating plants produce approximately 3.5 million cubic metres of bitumen per year, the solids flow associated with this production rate is 1/2 million tonnes per day (Sanders, 2004). Hydraulic transportation has been proved to be a viable technology for slurry transportation in a constrained mining environment. The original oil sand extraction processes applies belt conveyor to transport the mined ore, and a rotating inclined tumbler to liberate the bitumen from the sand. Large particles are not present in

the tailings stream as they are separated from the slurry at the tumbler outlet and transported to disposal sites by truck. Nowadays, belt conveyors have been replaced by oil sand hydrotransport operation. The ore is initially crushed and screened with a top size ranging between 50 and 150 mm. The crushed ore is then mixed with water, with lumps ablating and liberating oil to produce dense slurry. Considering its viability and efficiency in the oil sand extraction, slurry transport research has been sponsored by the industry for many years. Much of the research work has been conducted at the Saskatchewan Research Council's Pipe Flow Technology Centre in Saskatoon, SK (Sanders, 2004).

The oil sand industry currently utilizes mainly stationary pipeline for transporting minerals in most mines. In order to reduce the dependence on haulage truck for long haulage distances, there is a desire to extend the hydraulic transport system to production faces in oil sands mines using mobile pipeline systems. The mobile At Face Slurry System (AFSS) consists of a slurry production system on mobile units and flexible arrangement of pipelines, making it feasible to accept the feed from a large-capacity shovel. The ground articulating pipeline (GAP) system developed is capable to fold, extend and follow the excavators radially, horizontally and vertically. Oil sand converted to slurry at the mining face is delivered to a fixed pipeline by the GAP system.

1.2 Conceptual Design of the AFSS

The AFSS is intended to convert oil sands into slurry at mining faces and delivered to join a fixed pipeline via flexible GAP system. This concept requires innovative solutions to a complicated material handling need. Oil sands mechanical and chemical characteristics are demanded to be taken into consideration for the system design. A completed AFSS consists of one process platform working together with one pipeline system. For the processing platform, it would use a mixing tower to add water and size

material for pumping, or a large rotating tumbler to break up the oil sand material, with water added in the tumbler to create slurrified minerals. Shovel and mobile slurry system are directly connected to the folding pipeline system supported by tracked carbodies. The folding pipeline is a series of rigid trusses that carry slurry and water pipes. It forms the link between the processing platform and the fixed pipeline to the plant. Fresh water is carried on the flexible pipeline system to the processing platform, and the resulting slurry is carried back to the fixed pipeline for transport to the plant. Flexible pipeline is automatically controlled to follow the processing platform as needed anywhere during the mining operation. Sufficient flexibility should be achieved in order to meet the requirement. The folding pipeline system consists of a series of rigid truss frames that are allowed to swivel relative to each other. Truss joints at the end of each truss allow deflection to avoid torsional twist from the adjoining frames. A double ball joint is designed to permit the position change between adjacent trusses as well as to allow flow of both fresh water and oil sand slurry. The structure of the double ball joint is shown in Figure 1-1.

The unique ball joint assembly consists of an inner ball joint located inside an outer ball joint to allow the flow of slurry and fresh water. The ball joint should swivel around its vertical axis and flex longitudinally and laterally. The internal and external ball joints are co-axial as illustrated. An internal ball joint allows the flow of slurry while the external joint channels fresh water to produce oil sands slurry. Programmable control system or Global Positioning Satellite system is utilized to control track movement. It tells the track bodies the direction to follow the processing platform and the shovel.

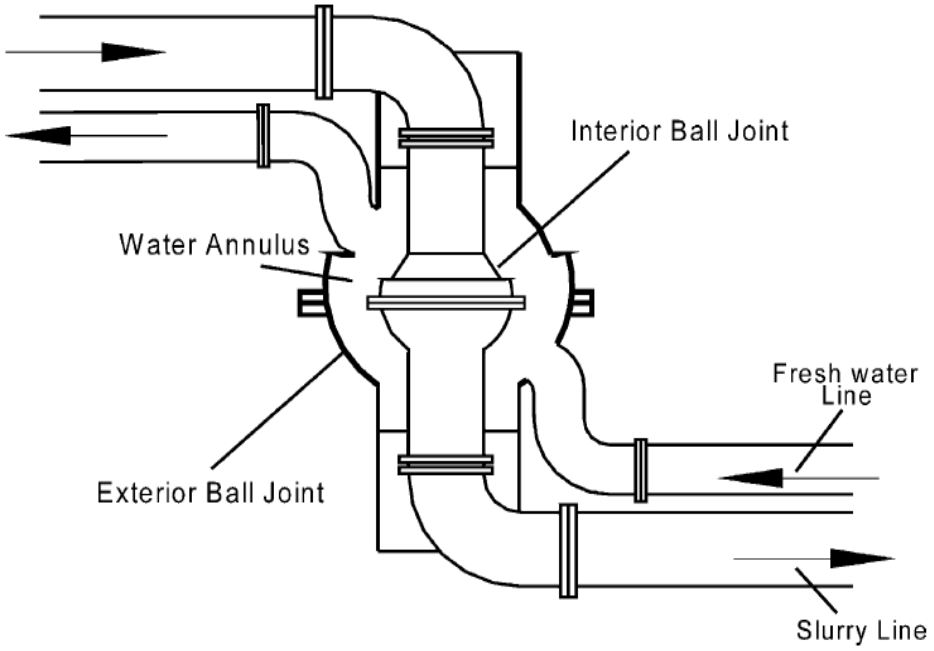

Figure 1-1 Double ball joint unit

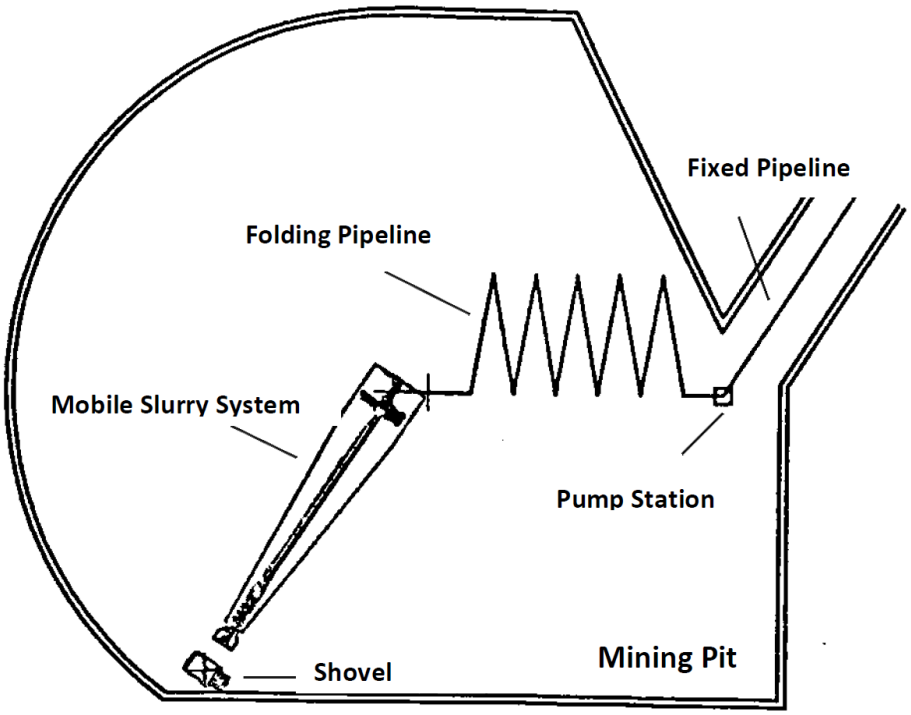

Figure 1-2 Conceptual design of AFSS

The operation concept of the AFSS is simply illustrated in Figure 1-2. A shovel dumps oil sand into the apron feeder, water is then added to produce oil sand slurry on the processing platform. Slurry is pumped through a connecting line to the flexible pipeline. The folding pipeline then transfer the slurry to the fixed pipeline connected directly to the plant. The folding pipeline has a minimum retracted length and a maximum extended length to enable the adjustment of the working length. A mining sequence will be established for the movement of the shovel within the pit, the design will allow the pipes to make zigzag movements and follow the shovels as needed at mining face.

1.3 Objectives and Scope of Study

AFSS concept has become a competitive means for materials handling toward the objective to optimize haulage system efficiency and cost. This mobile and flexible arrangement introduces a unique set of hydraulic transport problems. The scope of this thesis will focus to develop the mathematic models governing the friction and head losses with the AFSS concept and validate the model using data from Syncrude Canada Ltd. and Suncor Energy, Inc. via computational fluid dynamics (CFD) simulation.

2 Literature Review

2.1 Previous Research Work of Multiphase-Flows

2.1.1 Flow of Solid-Liquid Mixture in Pipe

Solid-liquid transportation has been widely used in the long-distance materials handling industry like coal, oil sand, and tailings. Many engineering models of slurry flow have been developed to predict and simulate frictional pressure loss and deposition velocity of "settling" slurries. Most of these models are phenomenological that they all require certain empirically derived parameters as input of the model and possess varying degrees of success in predicting the friction loss and deposition velocity. An initial empirical prediction model was developed by Durand (1953). It predicted the hydraulic gradients for coarse particle slurry flows. The model's calculation approach was improved by Wasp (1970) and applied to the commercial slurry pipeline design. Shook and Daniel (1968) later proposed a less complicated pseudo homogeneous approach to model slurry flow. This unique technique allowed description of the flow using a single set of conservation equations. The pseudo homogeneous approach had certain limitations as it assumed the slurry with no deposition velocity, which worked reasonably well for slurry with relatively fine particles, low solids volume fraction and a narrow range of operation velocities. The carrier fluid's density and viscosity were expected to increase with increasingly dispersed solid phase amount related to the in situ solids volume fraction. Considering the pseudo homogeneous approach's limitation, Shook and Daniel (1969) improved the model by considering the slurry as a pseudo single-phase fluid with variable density. However, the boundary conditions adopted in their approach made it difficult to apply to actual flow situations. An oversimplified model was proposed by Oroskar and Turian (1980), also known as "constructive energy" approach. The model was not intended for dense slurries and was used to calculate the deposition velocity. They

assumed that the kinetic energy of turbulent fluctuations was transferred to discrete particles, suspending them in the flow. This approach predicted deposition velocities reasonably well with the experimental data over a wide range of solids volume fractions. Based on previous research work, Wilson (1976) developed a one-dimensional two-layer model. The model assumed that the particles being very coarse were contained in the lower layer while upper layer's solids concentration being zero. The coarse-particle slurry flow consisted of two separate layers with each having a uniform concentration and velocity. Momentum transfer existed between the layers through interfacial shear forces. The two-layer model had been widely accepted and revised by many researchers. By assuming the lower layer to be stationary, Doron (1987) used the two-layer model for the prediction of flow patterns and pressure drops in slurry pipelines. However, failure to predict the existence of a stationary bed at low flow rates reduced the reliability of the friction loss predictions by this model. The dispersive force model developed by Wilson and Pugh (1988) was appropriate for predicting heterogeneous slurry flow, which made up for the limitations of pseudo homogeneous model. It took into consideration the particles suspended by fluid turbulence providing contact-load (Coulombic) friction and received extended applicability compared to the initial layer model by Wilson. Particle concentration and velocity profiles predicted using this model was in good agreement with experimental data. For a two layer slurry flow, slip characteristics and interaction between the layers demand detailed investigation. The most widely accepted two layer model is the SRC model developed by Gillies and co-workers (2004). The SRC two-layer model differs from the above phenomenological models since it does not depend on any empirically determined coefficients. On the contrary, effect of related parameters on friction loss is specified mechanistically. The model predicts pressure gradient and deposition velocity as a function of particle diameter, pipe diameter, solids volume fraction, and mixture velocity. Experiments for SRC two-layer model were mostly done

at the Saskatchewan Research Council Pipe Flow Technology Centre. Thousands of controlled experiments were conducted to obtain the semiempirical coefficients for the model. Data incorporated in the model was obtained at mixture velocities that were just greater than the deposition velocity ($V_c \leq V \leq 1.3V_c$) based on the fact that the optimum pipeline velocity being normally close to the Deposition velocity (V_c). By considering the existence of a dispersive layer sandwiching between the suspended layer and a bed, Doron and Barnea (1993) extended the two-layer modeling approach to a three-layer model for prediction of slurry low in horizontal pipelines. When the flow was in horizontal or near horizontal configurations, it was reasonable to assume a no-slip condition between the fluid and the solid parts. The dispersive layer displayed a higher concentration gradient outstripping the suspended layer. Satisfactory agreement with experimental data was achieved by the three-layer model. Transition lines between "flow patterns" also had drawn a lot of attention from researchers. Flow pattern maps essentially indicated the degree of flow heterogeneity. Doron and Barnea completed the flow pattern maps and determined the transition lines between the flow patterns based on a three-layer model. Solid-liquid slurry research work mentioned above is of great significance for the oil sand hydraulic transportation.

2.1.2 Flow of Oil Sand Slurry in Pipe

The oil sands slurry is a three-phase system that water, sand and bitumen phases co-exist with their superimposed behaviors affecting the entire system rheology (Noda, 1972). Frimpong (2003) conducted computational simulation of oil sand flow under steady-state conditions. Based on his previous work, he introduced higher level of complexity and relaxed some of the assumptions underlying the previous study. Frimpong (2010) simulated the system as an unsteady state model by incorporating the conditions for the flow system to evolve over time as it progressed from the initial steady condition to

unsteady flow situation. Multiphase flow modeling is very challenging. It becomes more complex with the introduction of the flexible at face slurry system. Due to its complexity, solutions of multiphase problems demand certain assumptions for reasonable simplification to yield tractable equations more effectively. According to Frimpong's work, following assumptions apply to the simulated unsteady-state oil sand slurry flow: (1) the flow is transient three-phase incompressible flow containing immiscible phases of hot water, oil, and solid sand. Air trapped is neglected; (2) the three-phase can be simply regarded as a liquid-solid two-phase model with oil and water combing to form a pseudo single fluid phase. Properties of oil and water are averaged into a single-phase component liquid phase; (3) no-slip condition is assumed between the phases. Solid particles are completely dispersed or suspended and carried continuously in the slurry; (4) adequate energy is provided by centrifugal pump that slurry velocity is above minimum deposition velocity. Sand particles are fully dispersed and no stationary bed exists at the bottom along the pipe length; (5) the pseudo single fluid phase is regarded as a continuous phase. Bitumen is a viscous fluid with high viscosity, but the existence of hot water reduces bitumen viscosity to a continuous viscous fluid (Frimpong, 2004); (6) the slurry temperature is assumed to be constant through the pipe length isothermal condition ; (7) solid particles are approximately spherical with a median diameter; (8) mixture properties: solid particles density of 2,650 kg/m3, bitumen API 10° and density of 995 kg/m3 and water/hot water density of 1,000 kg/m3 (McDonell, 2002); (9) flow rates and volume fractions of the phases are assumed to remain steady along the pipe length; (11) outlet pressure of pipe equals to the standard atmospheric value. Frimpong's work provided a further step toward a more realistic modeling of flexible-pipe system. Oluyemi (2011) provided more insight into oil sand multiphase flow in horizontal and inclined pipe configurations under a low sand loading. A steady-state turbulent flow simulation of this complex oil-sand-water-gas multiphase fluid was conducted using commercial CFD

software FLUENT. Most of the deep water reservoirs contained friable unconsolidated rocks. Sand in horizontal and deviated well would settle in the flow line depending on the flow parameters and pipe orientation. Deposited sand would directly result in reduction of the cross sectional area of the wellbore or pipe available for fluid flow. Industry's approach to managing sand deposition was to keep the carrier fluid velocity above the minimum transport velocity. The pressure drop mechanism in various pipe configurations was investigated by Oluyemi for a specified sand particle size and loading limit. Results indicated that sand deposited on the internal surface of pipe formed an extra layer of material at low sand loading, which led to increased pipe roughness and observed pressure drop.

2.2 Pressure Drop of Multiphase-Flows in Pipe

2.2.1 Pressure Drop of Solid-Liquid Slurry

2.2.1.1 The SRC Model

Pipeline friction losses are of great concern during slurry transportation. Slurry flows are normally divided into two categories in predicting pipeline friction losses. The two categories are non-settling or homogeneous flows and settling or heterogeneous flows, respectively. The first category is also occasionally denoted as pseudo homogeneous flow. The diameters of the particles in non-settling slurries are very fine and stationary bed is not expected to occur along the pipe length at low velocities. Pipeline flow patterns of the first category may be either laminar or turbulent with solid particles distributed uniformly in the carrier fluid at all velocities. A non-Newtonian fluid model is suitable for description of the flow characteristics of non-settling flow. The second category presents a more complicated flow pattern contrary to the homogeneous flow. With the presence of large diameter particles, stationary deposits will usually form at low velocities. The

heterogeneous flows are usually turbulent, with concentration distribution being less uniform and velocity distribution asymmetric.

As mentioned above, the most widely accepted two-layer model for predicting friction loss is the SRC model developed by Gillies and co-workers (2004). Gillies developed the most recent version of the SRC model based on slurry tests with high solids concentration. Data incorporated in their SRC model is obtained at velocity close to the deposition velocity. Wilson (2000) proposed that particles may experience a lift force repelling them from the wall and this repulsion can lead to reduced friction at high velocities. Gillies (2004) then conducted experiments to investigate this repulsion effect and incorporated it in the SRC model.

The particle adjacent to the pipe wall would experience the lift force in high velocity slurry flows. Wilson (2000) derived an expression to express this lift force to explain the repulsion effect that reduced the friction in high velocity slurry flows. This lift force was generated due to a portion of the particle projects beyond the viscous sub-layer and into the non-linear fluid velocity distribution region. Lift force investigated here neglected the effect of particles smaller than the viscous sub-layer. Friction between particle and wall would decrease with the parameter d^+ as a result of the lift force. d^+ was expressed as,

$$\mathrm{d}^+ = \mathrm{d}\rho_f u^*/\mu_f \qquad (2\text{-}1)$$

Where

d^+	Dimensionless particle diameter
d	Median particle diameter, (m)
ρ_f	Fluid density (kg/m^3)
u*	The friction velocity $(\tau_w/\rho_f)^{0.5}$ (m/s)

τ_w Wall shear stress, (Pa)

μ_f Fluid viscosity (Pa·s)

The SRC model had assumed a constant coefficient of Coulombic friction η_s relating normal and shearing stresses at the pipe wall:

$$\eta_s = \frac{\tau_s}{\sigma_s} \tag{2-2}$$

σ_s was resulted from the unsuspended portion of the immersed weight of the particles by lift forces. A constant friction coefficient was assumed under the condition that the fluid suspending forces being ineffective and presence of high solids concentration near the bottom of the pipe or channel. However, solid concentration near the bottom of the pipe may decrease prominently when fluid suspension was effective, which should be considered and incorporated into the SRC model. The SRC model retained the basic assumption that the friction coefficient was constant with certain correction of its variation effect, as Prasad's research had shown that the coefficient of friction increased as the solids concentration decreased based on their experiments conducted with a rotary shear apparatus (Prasad, 1995). Conceptual basis of the SRC model was illustrated in Figure 2-1.

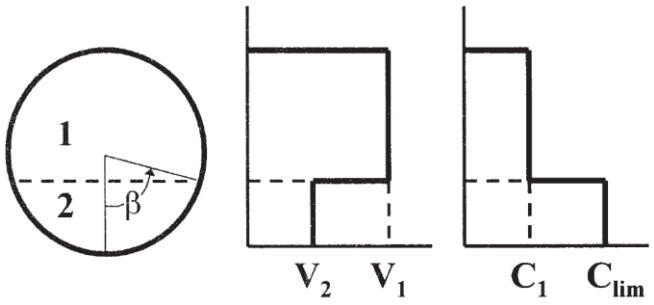

Figure 2-1 Idealized concentration and velocity distribution used in the SRC two-layer model (after Gillies, 2004)

Particles concentrated in the lower layer resulted in the Coulombic friction. The rest of particles were suspended by turbulence and distributed uniformly throughout the flow. This phenomenon contributed to the velocity and concentration distributing as step function. C_{lim}, the value calculated at (y/D = 0.15) using the method of Shook et al. (2002), represented the total concentration in the lower layer. The concentration of suspended particles C_1 was denoted as,

$$C_1 = C_r - C_c \tag{2-3}$$

Where Cr was the total in-situ solids concentration and Cc was the fraction that contributed Coulombic (contact load) friction. An empirical equation based on experimental pressure gradient measurements was used to calculate the ratio (C_c / C_r). This empirical equation has undergone changes as the model evolves to better understand the factors that govern wall friction. The equation for axial pressure gradient in horizontal flow was expressed as,

$$\frac{dP}{dZ} = \frac{\tau_1 S_1 + \tau_2 S_2 + F_2}{A} \tag{2-4}$$

Where

S Partial perimeter (m)

Z Axial distance, (m)

τ Shear stress, (Pa)

1 upper layer; 2 lower layer

A Cross-sectional area of pipe, (m^2)

Wilson's approach was used to calculate the Coulombic wall force F_2, this frictional force was resulted from the concentration difference ($C_{lim} - C_1$):

$$F_2 = \frac{0.5 g D^2 (\rho_s - \rho_f)(1 - C_{lim})(C_{lim} - C_1)(\sin\beta - \beta \sin\beta)\eta_s}{1 - C_{lim} + C_1} \tag{2-5}$$

β was the angle defined by the cross-sectional area of the lower layer:

$$A_2 = 0.5 D^2 (\beta - \sin\beta \cos\beta) \tag{2-6}$$

Stress τ_1 and τ_2 were dependent on the velocity and were calculated based on the velocity of the respective layers. Equation used for calculating the stress was as follows,

$$\tau_i = 0.5\, V_i^2 \left(f_{fi}\rho_f + f_{si}\rho_s\right) \tag{2-7}$$

Fluid Reynolds number and the wall roughness provided the basis for calculating the fluid friction factor f_{fi}, while the particle friction factor f_{si} turned out to be a function of the linear concentration λ_1 according to Gillies and Shook (2000), the linear concentration λ was expressed as,

$$\lambda = \left[\left(\frac{C}{C_{max}}\right)^{\frac{1}{3}} - 1\right]^{-1} \tag{2-8}$$

Where C was solids concentration, (volume fraction), C_{max} was settled deposit concentration (volume fraction). Based on the most recent version of SRC model mentioned above, Gillies and Shook conducted experiments in a closed loop pipeline of internal diameter 0.103 m, using sands with median diameters 0.09 and 0.27 mm. Pressure drops were measured under different slurry velocities and concentrations. Mean in-situ concentration *Cr* for each experiment was selected by adding weighed quantities of sand to the loop in a stepwise manner, whose initial volume was known. They proposed a new correlation for the particle friction factor that being used to modify the contact load fraction expression in the SRC model in predicting the pressure drop of heterogeneous slurry flows. Results obtained indicated that pipeline friction to be lower than expected at high velocities for slurries of sands with particle diameters of 0.09 mm and 0.27 mm, and the forces acting on particles in the near-wall region demanded further investigation.

The SRC two-layer model provides accurate predictions of frictional pressure drop and deposition velocity over a wide range of pipe diameter, particle size, particle

concentration under different slurry velocity, but it has certain limitations. The SRC model provides no detailed information about fluid turbulence, local particle velocities, or local particle concentrations, and is limited in application to straight runs of pipeline having a circular cross-sectional area or other complex geometries for slurry transportation (Kalekudithi, 2009). Kalekudithi (2009) launched a hydrodynamic simulation of horizontal slurry pipeline flow using ANSYS-CFX based on the kinetic theory of granular flow in view of these limitations. Computational Fluid Dynamics (CFD) is very promising in modeling hydrodynamics with the advent of increased computational capabilities. It is fully capable to simulate the single-phase flows, and is currently developing for modelling multiphase systems. The kinetic theory component of the CFD model takes into account the effects of the interactions between solid-solid phased and solid-liquid phase. Kalekudithi carried out simulation to investigate the effect of solids volume fraction, particle size, mixture velocity, and pipe diameter on spatial variations of particle concentrations and frictional pressure losses. The simulated data was then compared with existing experimental data over a wide range of pipeline operating conditions. Most of the existing experimental data were obtained with average solids concentrations ranging from 8 to 45% (by volume), median particle sizes ranging from 90 to 500 μm, slurry mixture velocities ranging from 1.5 to 5.5 m/s, and pipe diameters ranging from 50 to 500 mm. The predicted pressure drop was reasonably agreed with the experimental data. The comparison of predicted frictional pressure drop and experimental results over these wide range of pipeline operating conditions is shown in Figure 2-2.

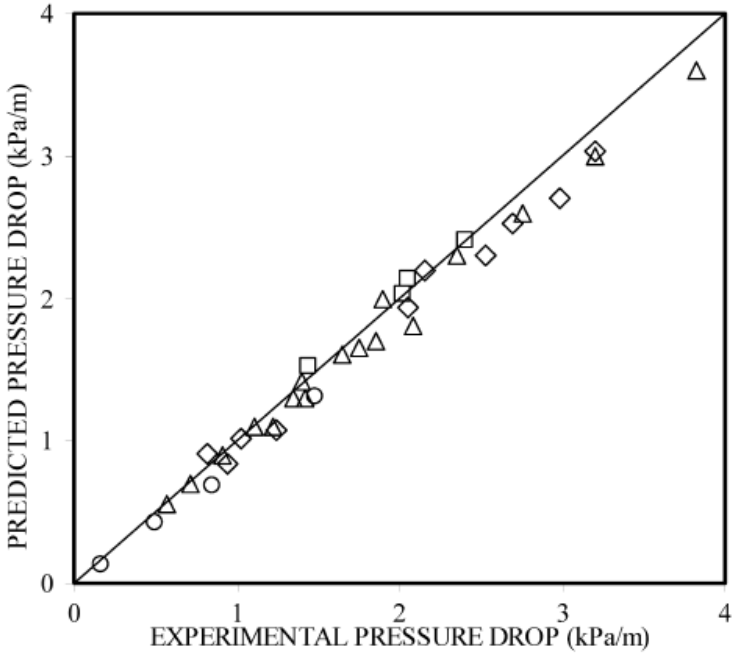

Figure 2-2 Parity plot for frictional pressure gradient compared to experimental data from Schaan et al.; Gillies and Shook; Gillies et al.; and Kaushal (after Kalekudithi, 2009)

2.2.2 Pressure Drop of Oil Sand Flow in Pipeline

Pressure drop is of great concern for oil sand slurry transportation. SRC Two-Layer model has been used to predict deposition velocities and pressure drops in oil sand industry. Much of this research has been conducted at the Saskatchewan Research Council's Pipe Flow Technology Centre in Saskatoon, SK (Sanders, 2004). However, as the limitations mentioned above, the SRC Two-Layer model does not account for the friction associated with the presence of large particles, and their effect on frictional pressure loss remains unknown. Seldom research has investigated the effect of large particles on slurry transportation. Presence of large particles, or lumps, may require a high slurry velocity to prevent its deposition and produce pressure drop measurements that are greater than the predicted data. Besides the effect of large particles,

hydrodynamic roughness of the pipe walls and presence of a stationary bed need to be considered to analyze the pressure drop of oil sand slurry pipelines. The hydrodynamic roughness of the pipe walls would increase if the walls are coated with bitumen or decrease if the walls have been smoothed from abrasion by sand particles (Sanders, 2000). Sanders initiated a quantitative analysis of the effects combining lumps, hydrodynamic roughness and the presence of a stationary bed on oil sand slurry friction losses. The pipelines considered in the study represented some of the most important hydrotransport applications in the oil sand industry. Most of these pipelines were substantially horizontal or contained sloped sections of considerable length, with sand being the primary solids component accounting for up to 60% (mass fraction).

Pressure drop is influenced by many independent variables like velocity, slurry density, pipe diameter and particle size distribution, etc. The fines fraction and the median particle size are the two most important particle size distribution (PSD) parameters in hydrodynamic transportation. The fines fraction determines the viscosity of the fines-water mixture that provides the carrier fluid for large particles. Typical size distributions have been reported by Sanders (Sanders, 2000). The conventional definition of fines employed in the oil sand slurry industry is 44 mm. However, the most recent version of the SRC Two-layer model also regards the 74 mm particles as fines fraction. The median particle size defined in the SRC Two-Layer differs from the regularly used median particle size as determined from a core sample (d_{50}). The median particle size defined in the SRC Two-Layer is denoted as d_{SRC}, which is the median of the +74 mm particles.

Sanders investigated the friction loss of five pipelines including two normal tailings pipelines, one hydro cyclone underflow pipeline, and two oil sand hydrotransport

pipelines. Figure 2-3 shows the friction pressure losses for water flow in one oil sand hydrotransport pipeline (D = 0.737 m) and one normal tailings pipeline (D = 0.737 m).

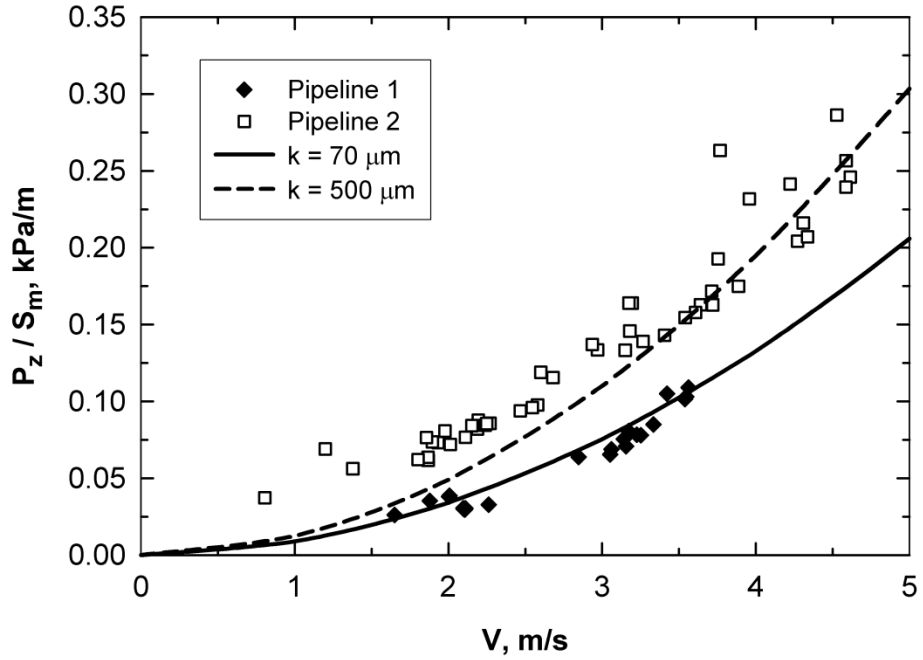

Figure 2-3 Friction pressure losses for water flow in oil sand hydrotransport pipeline (D = 0.737 m) and normal tailings pipeline (D = 0.737 m) (after Sanders, 2004)

Because of the presence of deposits and different pipe wall roughness, each pipeline presented a unique water friction locus. The influence of these factors on friction loss was investigated. Friction loss data during water flushing was collected and compared to the data simulated by the SRC Two-Layer model. Discrepancy emerged between the friction pressure losses for slurry flows in the operating pipelines and predicted by the SRC Two-Layer model. When assuming the particle size distribution being the same as that provided by analysis of the core samples, operational data was always greater than the correspondingly predicted one. Presence of large particles and/or stationary deposits may have contributed to this discrepancy. The deviation was more pronounced for pipelines containing inclined sections than those primarily horizontal pipelines. Figure 2-4 shows

the friction pressure losses for pipeline (oil sand hydrotransport, D = 0.737 m). The curves show SRC Two-Layer model predictions for 'Typical' slurry (specific gravity 1.50; roughness 70 μm; d_{SRC} 0.18 mm and viscosity 0.003 Pa·s) and 'Coarse' slurry (specific gravity 1.50; roughness 70 μm; d_{SRC} 0.40 mm and viscosity 0.002 Pa·s). Sanders recommended that the effect of pipe inclination on friction and a model to predict friction losses for slurries containing large particles should be developed.

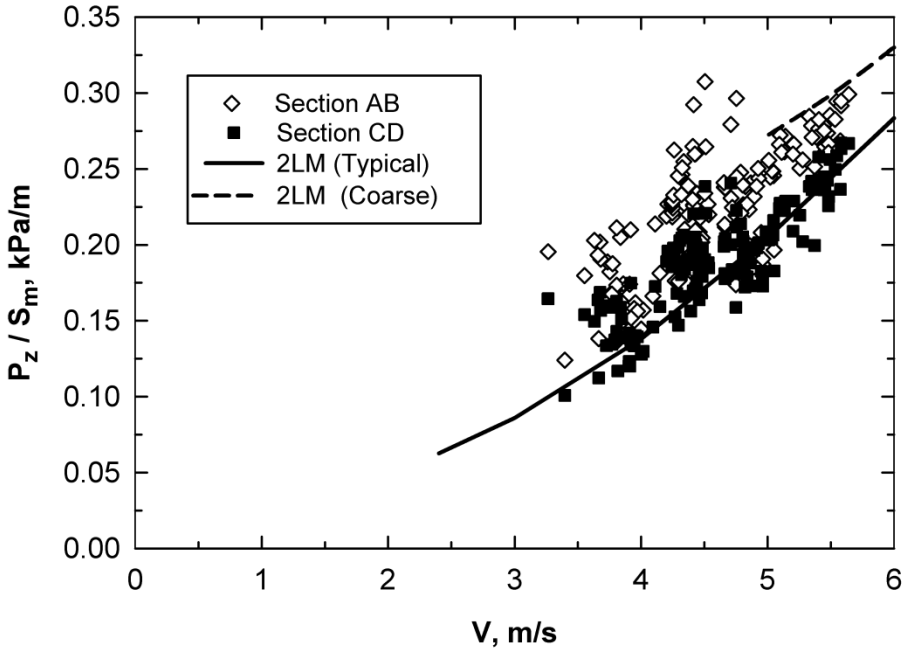

Figure 2-4 SRC Two-Layer model predictions for oil sand 'Typical' slurry (specific gravity 1.50; roughness 70 μm; d_{SRC} 0.18 mm, viscosity 0.003 Pa·s) and 'Coarse' slurry (specific gravity 1.50; roughness 70 μm; d_{SRC} 0.40 mm, viscosity 0.002 Pa·s) (after Sanders, 2004)

2.2.3 Effect of 90 Degree Bend on Pressure Drop

2.2.3.1 Effect of Bend on Single-Phase Flow

As mentioned in Chapter one, pipe arm systems of the AFSS must be connected together with flexible double ball joints in each pipe section that allows flow of both fresh water and slurry. For the convenience of research, pressure drop of only slurry flow is considered in this paper, the double ball joint of the AFSS then can be simplified as a model as shown in Figure 2-5, denominated as a swivel joint unit. The unit contains a vertical pipe section and two 90^{o} elbows with r/d = 1.5. The two elbows should swivel around the vertical axis of the vertical pipe section to allow the pipes making zigzag movements.

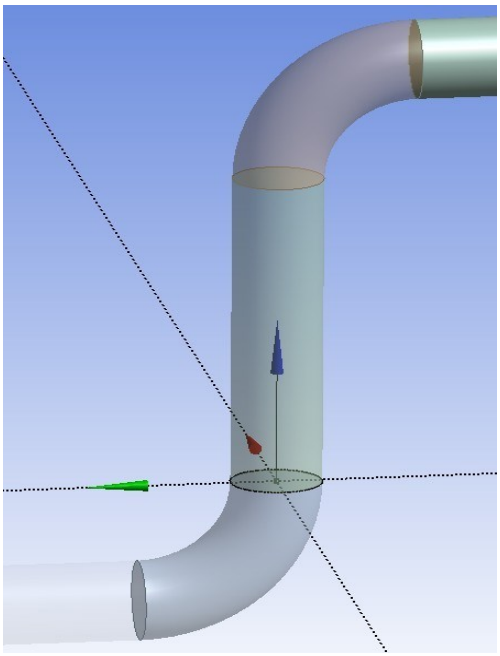

Figure 2-5 The simplified swivel joint unit model of the AFSS's double ball joint for slurry flow

For flow through a bend, the centrifugal force acting on the fluid produces a radial pressure gradient. A double spiral flow field is created by the fluid at the center of the pipe moving towards the outer edge and coming back along the wall towards the inner

edge because of the radial pressure gradient. Figure 2-6 shows the double spiral flow field. A large increase in pressure losses will probably be resulted from the bend curvature if it is strong enough, since flow separation may occur at these locations due to the adverse pressure gradient near the outer wall in the bend and near the inner wall after the bend. Rowe' data (1970), as shown in Figure 2-7, clearly illustrates the severe distortion effect of the bend in the flow field, even for fairly large-radius bends.

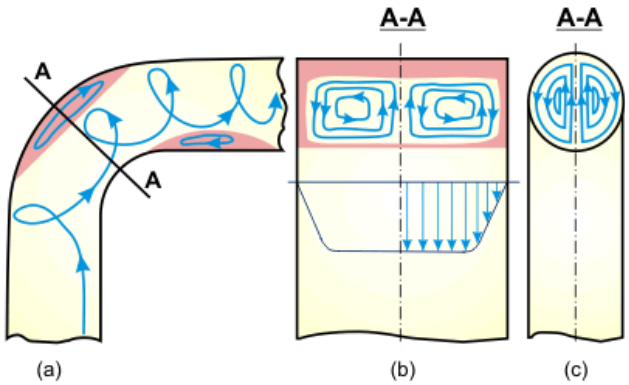

Figure 2-6 Schematic diagram of a double spiral flow in a bend: a) longitudinal section; b) cross-section; (c) cross-section (circular cross-section) (after Idelchik, 1986)

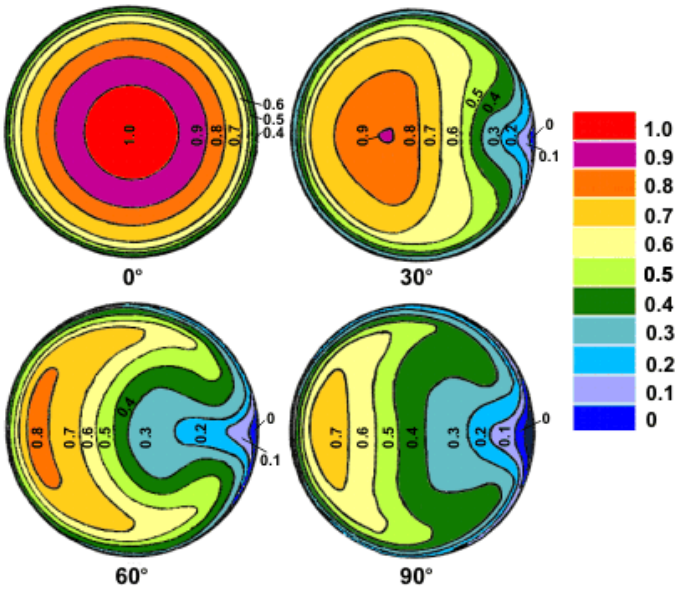

Figure 2-7 Total pressure contours in a U-bend of a bend-to-pipe diameter ratio of 24; Reynolds number = 236000 (after Rowe, 1970).

The change in the direction of flow in a bend causes pressure losses by both friction and momentum exchanges. Factors including bend angle, the curvature ratio and the Reynolds Number, they all have a significant impact on pressure loss. The overall pressure drop is equal to the sum of two components: 1) pressure drop resulted from friction in a straight pipe of equivalent length depending mainly on the Reynolds number; and 2) friction losses resulted from change of direction depending mainly on the curvature ratio and the bend angle, it can be normally expressed in terms of a bend-loss coefficient. Extensive data on loss coefficient for bends are given by Idelchik (1986).The single-phase pressure loss in a bend can thus be calculated as:

$$\Delta P = \frac{1}{2} f_s \, \rho \mu^2 \frac{\pi R_b}{D} \frac{\theta}{180^o} + \frac{1}{2} k_b \, \rho \mu^2 \tag{2-9}$$

Where *fs* is the Moody friction factor in a straight pipe; ρ, the density; u, the mean flow velocity; R_b the bend radius; D, the tube diameter; θ, the bend angle; and k_b, the bend loss coefficient obtained from Figure 2-8.

Flow in pipe bend could also be characterized by the Dean number D_e (Dean, 1928). The Dean number can be defined in terms of pipe diameter D or the center-line bend radius R. It governs the relative importance of viscous, inertia and curvature terms, which is represented by the ratio of the product of the inertia and centrifugal forces to the viscous forces. The equation is expressed as,

$$D_e = \left(\frac{dv\rho}{\mu}\right)\left(\frac{r}{R}\right)^{\frac{1}{2}} \tag{2-10}$$

Where d is pipe diameter, v is velocity, ρ is density, μ is dynamic viscosity, r is pipe radius and R is pipe bend center-line radius.

A typical 90^{o} bend is shown in Figure 2-9. We denoted point A on the surface of the bend outer wall and point B at the inside surface of the bend.

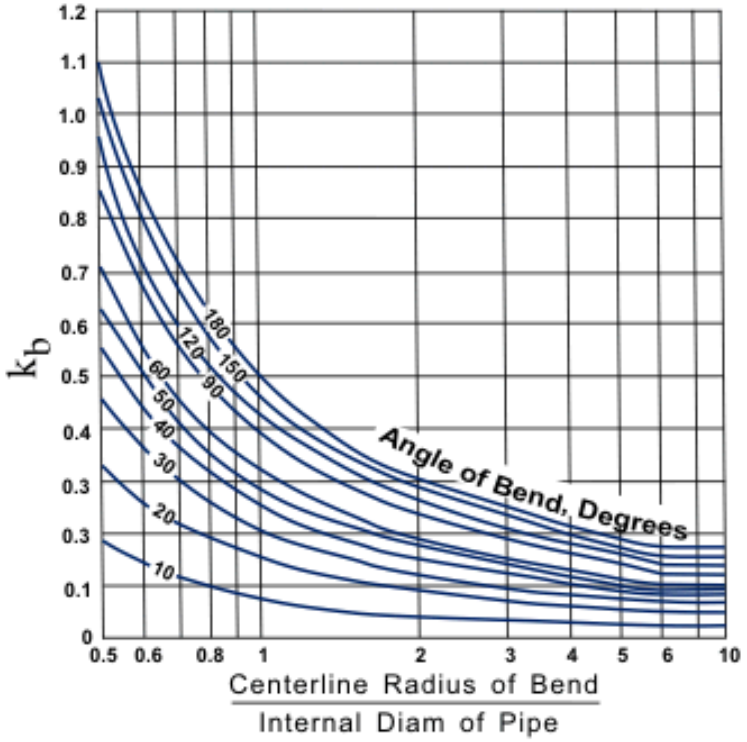

Figure 2-8 Bend loss coefficients for a pipe (after Babcock & Wilcox Co., 1978)

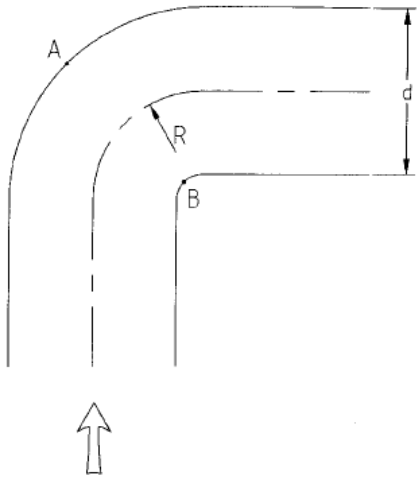

Figure 2-9 A typical pipe bend

The pressure drop for bend can defined in terms of head loss coefficient K or the equivalent pipe length L_e. According to Crawford (2003), two separate effects combined together and resulted in the bend pressure drop. As fluid flows around the bend, it would encounter the pressure gradient and led to excess friction around point A. This effect is denoted as the adverse pressure gradient at the outer wall. The second effect is resulted from the secondary flow that aroused due to the geometry of the bend. The flow separates from the pipe wall at the inside surface around point B. The value of *R/d* is critical to determine the significance of each effect. The bend is referred to as a curved pipe when *R/d* > 15 and as an elbow while below this value. Ito (1959) developed a model to describe the first effect for curved pipes at higher R/d values.

$$\mathrm{K}\left(\frac{D}{d}\right)^{0.5} = 0.00362 + 0.038\left[Re\left(\frac{d}{D}\right)^{2}\right]^{-0.25} \tag{2-11}$$

This effect also corresponded well with Mori and Nakayama's model (1967), which is expressed as,

$$\mathrm{K}\left(\frac{D}{d}\right)^{0.5} = 0.0375\left[Re\left(\frac{d}{D}\right)^{2}\right]^{-0.22} \times \left\{1 + 0.112\left[Re\left(\frac{d}{D}\right)^{2}\right]^{-0.2}\right\} \tag{2-12}$$

Where

$$\left(\frac{Le}{d}\right) = 19.8333 K Re^{0.25}\left(\frac{D}{d}\right) \tag{2-13}$$

Meanwhile the second effect of separation at the inner part of the bend could be predicted by the relation,

$$\left(\frac{Le}{d}\right) = 22.2126\left[Re\left(\frac{d}{D}\right)^{2}\right]^{0.7888} Re^{-0.71438} \tag{2-14}$$

Crawford compared the data predicted by these models with existing bend pressure drop data. It turned out that these equations could reasonably predict the bend pressure drop data over the turbulent range up to $Re = 3 \times 10^5$ within a spread of +3 to -2 percent.

Besides theoretical model evaluation of pressure drop, Computational fluid dynamics (CFD) is also very promising in modeling hydrodynamics with the advent of increased computational capabilities. CFD validation is also of great significance for both experimental work and empirical model prediction of bend pressure drop. CFD has been proved to be successful in simulating various kinds of engineering problems over the last 50 years. Ellison et al (1997) conducted experiments for air water through branching and developed a two-dimensional CFD model to predict the phase separation in branching junctions. A CFD code was developed by Hatziavramidis et al. (1997) to simulate the transient flow simulations of air-water and steam-water flows through branching and impacting T-junctions. Coffieldet al. (1997) used CFD analysis to study their recoverable pressure loss coefficients for two elbows in series. Wang and Shirazi (2001), Peniguel et al (2003), Guessous (2004), Song et al. (2004), Akilli et al. (2001), and Riffat and Gan (1997) all conducted research work and developed a 3D CFD model using an Eulerian continuum approach in conjunction with the k-ε turbulence model related to pipe fittings. A 3D CFD model had been constructed to simulate single-phase fluid flow in two commonly used pipe fittings: an elbow and a T-joint using the STAR-CD code by Moujaes (2006). The elbow and T-joint model used in Moujaes's research is shown in Figure 2-10.

Elbow model T-joint model

Figure 2-10 the elbow and T-joint model using SolidWorks Program

A variety of flow conditions with Re number ranging from 0.78×10^5 to 1.56×10^5 were simulated. Six uniformly distributed values of Re numbers were chosen within the above range. Flow reversal regions near the inner radius and high velocity regions near the outer radius downstream of the elbow were indicated based on the velocity profile. Pressure located on the outer radius was high and changed significantly to a low one on the inner radius. For the T-joint flow scenario, recirculation occurred immediately downstream of the elbows when flow into the center leg. Velocity was high just downstream from the stagnation zone. Significant pressure gradients existed across the flow area before the flow split into the two legs of the T-joint.

2.2.3.2 Effect of Bend on Multi-phases Flow

The research discussed above for bend is just for single-phase flow. However, two-phase or multiphase flow is constantly observed in many industries including petroleum, chemical, oil, and gas industries, etc. (Sanchez, 2010). Multiphase flow is defined as the simultaneous flow of several phases, with two-phase flow being the simplest case (Wallis, 1969). Due to the presence of different flow patterns, the equations governing two-phase flow are more complex than single-phase flow (Benbella, 2009). Friction factor and pressure drops have been investigated in several horizontal (Cole, 2004) and vertical (Kongkiatwanitch, 2001) two-phase and multiphase flows (Spedding, 2006). The two-phase flow typically produces an undesirable higher pressure drop compared to single-phase flow. Same as the single-phase flow in bend, secondary flow will be produced under the joint effect of centrifugal force and boundary layer at the wall. Centrifugal force is caused by the curvature of bend as fluid flows through the bend and then directed from the momentary center of the curvature toward the outer wall of the pipe. The undesirable high-pressure drop is difficult to predict due to the lack of a model for determining the two-phase flow through pipe components. Chisholm (1983) presented an

elementary model for prediction of two-phase flow in bends, where he introduced a liquid two-phase multiplier based on different pipe diameters, *r/d* values, and flow rates. According to Chisholm's model, stratification of the two phases was induced by the centrifugal force in the bend, making the two-phase flow in bends more complex. The normal practice to calculate two-phase pressure drop is to multiply the single phase pressure losses by a factor known as the empirically-correlated two-phase multiplier.

$$\frac{\Delta P_{TP}}{\Delta P_{LO}} = 1 + \left(\frac{\rho_L}{\rho_G} - 1\right) \times \left[\left\{1 + \frac{2.2}{k_{LO}\left(2+\frac{R_b}{D}\right)}\right\} \times (1 - x) + x^2\right] \quad (2\text{-}15)$$

Where ΔP_{TP} is the pressure drop in two-phase flow, ΔP_{LO} is pressure drop in a single phase flow of the total mass flux and liquid properties, k_{LO} is the bend loss coefficient for single phase flow, and x is the dry quality.

However, most of these two-phase pressure loss studies have been confined to the horizontal plane. Chenoweth and Martin (1955) adopted the Lockhart-Martinelli (1949) model to predict the two-phase pressure drop around bends, a model initially developed for straight pipe. The correlation turned out effective in predicting loss in bends and other pipe fittings. Fitzsimmons (1964) presented two-phase pressure loss data for bend in terms of the equivalent length and the ratio of the bend pressure loss to the straight pipe frictional pressure gradient. Sekoda et al. predicted the two-phase bend pressure drop using a two-phase multiplier, referred to as a single-phase liquid pressure loss in the bend. Results indicated that the two-phase pressure drop was dependent on the r/D ratio while independent of pipe diameters (Sekoda, 1969). Flow pattern also has an impact on the pressure drop for flow through 90 degree bend. Orientation of the plane of the bend giving contrary results has been reported by previous research work. Debold (1962)

declared that the same bend pressure loss was found in horizontal bend, the horizontal to vertical up-bend, and the vertical down to horizontal bend, but not the horizontal to vertical down-bend, which had a 35% less pressure drop than the other three. Debold's model correlating the elevation with pressure drop for the homogeneous model was assumed to be suitable for the two-phase flow. Alves (1954), though, completely ignored the influence of head pressure differences. Impact of flow patterns on pressure drop is complicated and uncertain that even opposite conclusions would be reached. Peshkin (1961) reported that horizontal to vertical down flow shows 10% greater pressure drop through bend than the corresponding horizontal to vertical up-flow case, while Kutateladze (1969) declared that the horizontal to vertical up-flow bend created more pressure drop. Moujaes and Aekula developed CFD models in HVAC pipes to investigate the effects of pressure drop on turning vanes in 90 degree duct elbows (Moujaes and Aekula, 2009). It can be seen that various approaches have been applied to predict pressure drop in elbows. Mazumder (2012) conducted CFD analysis of air-water two-phase flow in four different elbows based on the previous research work. His simulated results were validated using Azzi's (2005) and Chisholm's (1983) empirical models. Kumar conducted experiments to measure pressure drop of sand-water two-phase slurry flow through the pipe bend. Data was compared to the simulated result using commercial CFD package Fluent. Result indicated that the Eulerian two-phase model could reasonably predict the pressure drop with a slurry pipe bend in the horizontal plane. Pressure drop along the pipe bend increased with flow velocity and particle concentration. Pressure at the inner wall was less than that at the outer wall in the bend, the velocity and concentration distribution of solids became more uniform downstream.

2.3 Research Methodology and Structure of the Thesis

The At Face Slurry System introduces a unique set of hydraulic transport problems. Based on the previous research work mentioned above, SRC Two-Layer model has been used to predict deposition velocities and pressure drop of oil sand slurry in horizontal pipelines. Oil sand slurry flow in flexible pipeline and pipe bend has been scarcely investigated. Frimpong (2003) simulated the oil sand slurry flow in the ground articulating pipeline using finite difference equations and computer modeling. Computer simulation and experimentation of oil sand flow in AFSS urgently demand further research work. CFD is very promising in modeling hydrodynamics with the advent of increased computational capabilities and its more suitably finite volume approach compared to finite difference approach. The paper will focus to develop the mathematic models governing the friction and head losses with the AFSS concept. The research work is basically divided into three separate parts in this paper.

(1) Flow of oil sand slurry in horizontal pipeline is simulated using the commercial CFD package Ansys – Fluid dynamics – Fluent 14.5. Results are compared to field pressure drop data from Syncrude Canada, Ltd. and Suncor Energy, Inc.'s stationary pipeline system to develop a mathematic model suitable governing the friction loss for horizontal pipeline.

(2) A flexible arrangement of pipe loops capable of folding and extending imitating the AFSS concept are set up in the laboratory. Experimental and modelling results are obtained and compared to test the accuracy of CFD modelling to predict pressure drop in flexible pipeline system.

(3) Based on research work in the previous two parts, flow of oil sand slurry in the folding pipeline of the At Face Slurry System is simulated to validate its technical viability.

3 CFD Simulation of Oil Sand Slurry Flow in Pipe

3.1 CFD Basics of Multiphase Modelling

Appropriate physical and mathematical model is essential for CFD simulation. Finite element, finite volume and finite difference method are used to obtain a set of partial differential equations based on the mathematical model. Due to its inherent conservation, finite volume method is mostly applied in discrediting the partial differential equations. Navier-Stokes equations are commonly used to describe the state of flow and are generally solved for all flows in CFD modelling. The continuity and the momentum expression of Navier-Stokes equations are shown as (ANSYS CFX Solver Theory Guide, 2011),

$$\frac{\delta\rho}{\delta\tau} + \nabla \cdot (\rho u) = 0 \tag{3-1}$$

$$\frac{\delta\rho u}{\delta\tau} + \nabla \cdot (\rho u u) = -\nabla \mathrm{p} + \ + \nabla \cdot \tau + \rho g \tag{3-2}$$

Where ρ is density, u is instantaneous velocity, p is pressure, τ is the viscous stress tensor and g is the gravity vector. Full description of a flow may require additional equations, such as the energy equation and/or turbulence equations.

Direct numerical simulation (DNS) is a method to solve the governing equations without any modelling. However, this method is time-consuming and ineffective. Flows in most engineering problems are turbulent and would exhibit time scales of significantly different magnitudes. This demands fine mesh resolution, which makes the calculation become unfeasible. Effects of turbulence thus have been the main focus of single-phase CFD research for the last couple of years. Multiphase flow is even more complex than single-phase flow and demands more in-depth modelling due to the interaction between

different phases. Section 3.1 introduces some basics of multiphase flow and fundamental concepts of CFD multiphase model based on the Fluent User Guide (Fluent, 2003).

3.1.1 The Basic CFD Approach

Multiphase flow is constantly observed in many industries including petroleum, chemical, oil, and gas industries, etc. Physical phases of matter are gas, liquid and solid; however, in multiphase flow, a phase can be defined as an identifiable class of material that has a particular inertial response to and interaction with the flow and the potential field in which it is immersed (Fluent, 2003). For instance, Solid particles made of same material but with different diameters would be regarded as different phases based on the assumption that particles with the same size will have a similar dynamical response to the flow field. Multiphase flow can be grouped into four categories including gas-liquid or liquid-liquid flows, gas-solid flows, liquid-solid flows and three-phase flows. Advances in computational fluid dynamics technology allow further insight into the mechanism of multiphase flows. Two approaches are commonly used for the numerical calculation of multiphase flows: the Euler-Lagrange approach and the Euler-Euler approach.

3.1.1.1 The Euler-Lagrange Approach

The history of individual fluid particles is essentially tracked (Figure 3-1) in the Lagrangian approach. Flow variable F in Lagrangian description is expressed as a function of time, t, and the position vector of the particle at reference zero time, x_0. While the Eulerian description depicts the change of flow variables at a fixed spatial point, x, which is a function of both spatial position, x, and time, t. The Euler-Lagrange Approach tracks the particulates through the flow using Lagrangian description and describes the fluid in the Eulerian way. The fluid phase is regarded as a continuum by solving the time-averaged Navier-Stokes equations. The approach assumes that the dispersed second phase

occupies only a low volume fraction and is solved by tracking a large number of particles, bubbles, or droplets through the calculated flow field. Momentum, mass, and energy are interchangeable between the dispersed phase and fluid phase. Behavior of the particles in the flow could be tracked by integrating a set of ordinary differential equations in time for each sample particle. Since it is not realistic to track each particle even in dilute suspension, the full particulate phase is modeled by just a sample of individual particles (ANSYS, 2003). The Euler-Lagrange Approach is not applied in the CFD simulation of oil sand flow in this paper, so it is not introduced here.

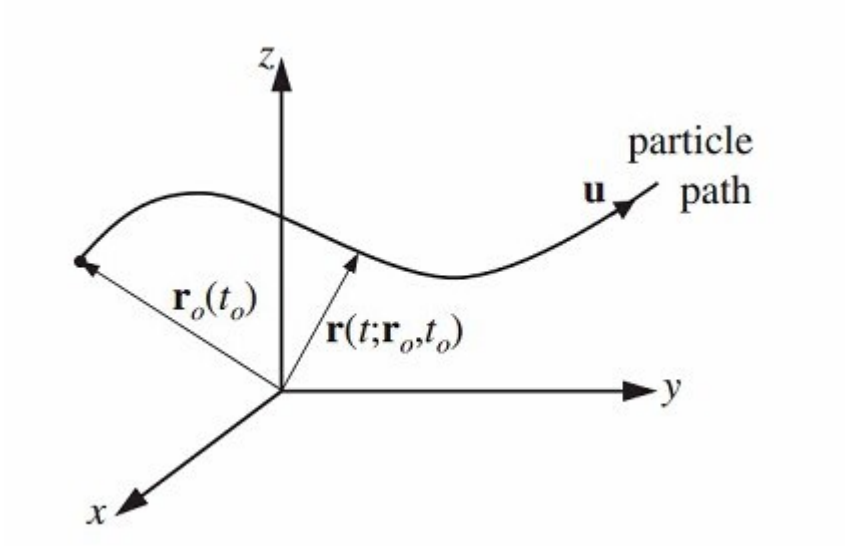

Figure 3-1 Lagrangian Description of Fluid Motion (after Kundu, 2002)

3.1.1.2 Euler-Euler Methods

For the purpose of simplifying the derivation of the hydrodynamic equations, phases in the Euler-Euler approach are treated mathematically as interpenetrating continua. The concept of phasic volume fraction is introduced in the approach. The computational domain is divided into control volumes where volume of a phase cannot be occupied by the other phases. Volume fractions of phases are expressed as continuous functions of space and time with their sum equal to one. The computational efforts of modeling the solid-liquid flow is significantly reduced by following the volume fraction of each phase,

especially the solid phase in each control volume instead of tracking each individual solid particle. Conservation equations with similar structure are derived for each phase. Constitutive relations obtained from empirical information are provided for closing these equations. The following section will introduce the details of these hydraulic equations and their closure.

3.1.2 General Hydrodynamic Equations for Multiphase Flow

The conservation equation can be derived by ensemble averaging the local instantaneous balance for each of the phase or by using the mixture theory approach (Syamlal, 1993). Phases in this approach are treated mathematically as interpenetrating continua. The portion of volume occupied by each phase in a control volume is described as the concept of phasic volume fractions α_q. Based on the concept that conservation equations should be satisfied by each phase individually, governing equations of conservation of mass and momentum are derived. The sum of volume fractions of all phases in any control volume equals to 1, as expressed as,

$$\sum_{q=1}^{n} \alpha_q = 1 \tag{3-3}$$

The volume of phase q, expressed as V_q, is calculated as,

$$V_q = \int_V \alpha_q dV \tag{3-4}$$

The effective density is expressed as

$$\widehat{\rho_q} = \alpha_q \rho_q \tag{3-5}$$

Where ρ_q is the physical density of phase q.

3.1.2.1 Continuity Equations

The continuity equation for phase q is

$$\frac{\partial}{\partial t}(\alpha_q \rho_q) + \nabla \cdot (\alpha_q \rho_q \vec{v}_q) = \sum_{p=1}^{n} \dot{m}_{pq} \tag{3-6}$$

Where $\vec{v}_q$ is the velocity of phase q and $\dot{m}_{pq}$ is the mass transfer from the p^{th} to q^{th} phase.

3.1.2.2 Conservation of Momentum

The conservation of momentum for a liquid phase q is

$$\frac{\partial}{\partial t}(\alpha_q \rho_q \vec{v}_q) + \nabla \cdot (\alpha_q \rho_q \vec{v}_q \vec{v}_q) = -\alpha_q \nabla p + \nabla \cdot \bar{\bar{\tau}}_q + \alpha_q \rho_q \vec{g}$$

$$+\alpha_q \rho_q (\vec{F}_q + \vec{F}_{lift,q} + \vec{F}_{vm,q}) \tag{3-7}$$

Where $\vec{g}$ is the acceleration due to gravity, $\bar{\bar{\tau}}_q$ is the q^{th} phase stress-strain tensor, p is the pressure, $\vec{F}_q$ is an external body force, $\vec{F}_{lift,q}$ is a lift force, and $\vec{F}_{vm,q}$ is a virtual mass force, K_{pq} is the momentum exchange coefficient between p^{th} and q^{th} phases. The term $\dot{m}_{pq}$ characterizes the mass transfer from p^{th} to q^{th} phase, $\vec{v}_{qp}$ is the relative velocity between q^{th} and p^{th} phase.

The conservation of momentum for s^{th} solid phase is,

$$\frac{\partial}{\partial t}(\alpha_s \rho_s \vec{v}_s) + \nabla \cdot (\alpha_s \rho_s \vec{v}_s \vec{v}_s) = -\alpha_s \nabla p - \nabla p_s + \nabla \cdot \bar{\bar{\tau}}_s + \alpha_s \rho_s \vec{g} +$$

$$\alpha_s \rho_s (\vec{F}_s + \vec{F}_{lift,s} + \vec{F}_{vm,s}) + \sum_{l=1}^{N} (\dot{m}_{ls} \vec{v}_s + K_{ls}(\vec{v}_l - \vec{v}_s)) \tag{3-8}$$

Where p_s is the s^{th} solids pressure, K_{ls} is the momentum exchange coefficient between fluid or solid phase l and solid phase s, N is the total number of phases. $\bar{\bar{\tau}}_s$ is the s^{th} phase stress-strain tensor, $\vec{F}_s$ is an external body force, $\vec{F}_{lift,s}$ is a lift force, and $\vec{F}_{vm,s}$ is a virtual mass force. K_{ls} is the momentum exchange coefficient between l^{th} and s^{th} phases. $\dot{m}_{ls}$ is the mass transfer from l^{th} to s^{th} phase, $\vec{v}_{ls}$ is the relative velocity between l^{th} and s^{th} phase.

3.1.2.3 Closure of Momentum Conservation Equation

As shown in the above momentum conservation equations, it is necessary to determine the solid shear stress, fluid shear stress as well as momentum exchanges between solid and fluid and between solid and solid phase. The formulations for liquid-solid momentum transfer and solid-solid momentum transfer are briefed for the CFD commercial package Fluent.

(A) Fluid Stress Tensor

In Fluent, the fluid viscous stress tensor,$\bar{\bar{\tau}}_g$ is assumed to be of Newtonian form:

$$\bar{\bar{\tau}}_g = 2\alpha_g\mu_g\bar{\bar{D}}_g + \alpha_g\lambda_g tr(\bar{\bar{D}}_g)\bar{\bar{I}} \tag{3-9}$$

where $\bar{\bar{D}}_g$ is the strain tensor for fluid phase, μ_g and λ_g are dynamic viscosity and bulk viscosity for fluid phase.

(B) Fluid-Solid Momentum Exchange Coefficient

The fluid-solid exchange coefficient is expressed as,

$$K_{sl} = \frac{\alpha_s\rho_s f}{\tau_s} \tag{3-10}$$

where drag function, f, is defined differently for the different exchange-coefficient models,τ_s, the particulate relaxation time, is defined as

$$\tau_s = \frac{\rho_s d_s^2}{18\mu_l} \tag{3-11}$$

where d_s is the diameter of particles of phase *s*.

Fluent package contains different drag function models. Drag function *f* has different expressions in these models and may include drag coefficient based on the relative Reynolds number. Details of these models are introduced below.

- Syamlal-O'Brien Model

$$f = \frac{C_D Re_s \alpha_l}{24 v_{r,s}^2} \tag{3-12}$$

Dalla Valle derives the equation of drag coefficient C_D, where C_D is expressed as,

$$C_D = \left(0.63 + \frac{4.8}{\sqrt{\frac{Re_s}{v_{r,s}}}}\right)^2 \tag{3-13}$$

Where Re_s is defined as

$$Re_s = \frac{\rho_l d_s |\vec{v}_s - \vec{v}_l|}{\mu_l} \tag{3-14}$$

Where the subscript *l* is for the l^{th} fluid phase, *s* is for the s^{th} solid phase, and d_s is the diameter of the s^{th} solid phase particles. The terminal velocity correlation for the solid phase is

$$v_{r,s} = 0.5\left(A - 0.06Re_s + \sqrt{(0.06Re_s)^2 + 0.12Re_s(2B - A) + A^2}\right) \tag{3-15}$$

Where $A = \alpha_l^{4.14}$ and $B = 0.8\alpha_l^{1.28}$ for $\alpha_l \leq 0.85$ and $B = \alpha_l^{2.65}$ for $\alpha_l > 0.85$.

This model is appropriate when the solid shear stresses are defined according to (Syamlal, 1993)

- Wen and Yu Model

The solid-liquid exchange coefficient is of the following form:

$$K_{sl} = \frac{3}{4} C_D \frac{\alpha_s \alpha_l \rho_s |\vec{v}_s - \vec{v}_l|}{d_s} \alpha_l^{-2.65} \tag{3-16}$$

Where the drag coefficient

$$C_D = \frac{24}{\alpha_l Re_s}[1 + 0.15(\alpha_l Re_s)^{0.687}] \quad (3\text{-}17)$$

This model is appropriate for dilute systems.

- Gidaspow Model

This model is a combination of the Wen and Yu model and the Ergun equation.

When $\alpha_l > 0.8$, the fluid-solid exchange coefficient K_{sl} is expressed as:

$$K_{sl} = \frac{3}{4} C_D \frac{\alpha_s \alpha_l \rho_s |\vec{v}_s - \vec{v}_l|}{d_s} \alpha_l^{-2.65} \quad (3\text{-}18)$$

Where

$$C_D = \frac{24}{\alpha_l Re_s}[1 + 0.15(\alpha_l Re_s)^{0.687}] \quad (3\text{-}19)$$

When $\alpha_l \leq 0.8$,

$$K_{sl} = 150 \frac{\alpha_s (1-\alpha_l)\mu_l}{\alpha_l d_s^2} + 1.75 \frac{\rho_l \alpha_s |\vec{v}_s - \vec{v}_l|}{d_s} \quad (3\text{-}20)$$

This model is recommended for dense fluidized beds.

(C) Solid Pressure and Solid Stress Tensor

(a) Solid pressure

For granular flows in the compressible regime (i.e., where the solids volume fraction is less than its maximum allowed value, a solid pressure is calculated independently and used for the pressure gradient term, ∇P_s, in the granular phase momentum equation. Due to the fact that a Maxwellian velocity distribution is used for the particles, a granular temperature is introduced into the model, and appears in the expression for the solids pressure and viscosities. The solids pressure is composed of a kinetic term and a second term due to particle collisions:

$$p_s = \alpha_s \rho_s \Theta_S + 2\rho_s(1 + e_{ss})\alpha_s^2 g_{0,ss}\Theta_S \quad (3\text{-}21)$$

Where e_{ss} is the coefficient of restitution for particle collisions, $g_{0,ss}$ is the radial distribution function, and Θ_S is the granular temperature. *FLUENT* uses a default value of 0.9 for e_{ss}, but the value can be adjusted to suit the particle type. The granular temperature Θ_S is proportional to the kinetic energy of the fluctuating particle motion. The function$g_{0,ss}$is a distribution function that governs the transition from the compressible condition with$\alpha < \alpha_{s,max}$, where the spacing betweenthe solid particles can continue to decrease, to the incompressible condition with$\alpha = \alpha_{s,max}$, where no further decrease in the spacing can occur.

Radial Distribution Function, g_0, is a correction factor that modifies the probability of collisions between grains when the solid granular phase becomes dense. This function may be regarded as the non-dimensional distance between spheres:

$$g_0 = \frac{s + d_p}{s} \quad (3\text{-}22)$$

Where s is the distance between grains, *FLUENT* implemented the radial distribution function proposed by Ranz (1958):

$$g_0 = \left[1 - \left(\frac{\alpha_s}{\alpha_{s,max}}\right)^{1/3}\right]^{-1} \quad (3\text{-}23)$$

If the number of solid phase is greater than 1, the radial distribution function is extended to

$$g_{0.ll} = \left[1 - \left(\frac{\alpha_l}{\alpha_{l,max}}\right)^{1/3}\right]^{-1} \quad (3\text{-}24)$$

Where $\alpha_{l,max}$ is specified during the problem setup, and

$$g_{0,lm} = \frac{d_m g_{0,ll} + d_l g_{0,mm}}{d_m + d_l} \tag{3-25}$$

(b) Solid shear stress

The solid shear stress tensor appears in the liquid-solid momentum equations. It contains shear and bulk viscosities arising from particle momentum exchange due to translation and collision. A friction component of viscosity can be included to account for the viscous-plastic transition that occurs when particles of a solid phase reach the maximum solid volume fraction.

The solid shear viscosity is the sum of the collisional and kinetic parts, and the optional friction part:

$$\mu_s = \mu_{s.col} + \mu_{s,kin} + \mu_{s,fr} \tag{3-26}$$

(b.1) Collisional Viscosity

$$\mu_{s,col} = \frac{4}{5}\alpha_s \rho_s d_s g_{0,ss}(1 + e_{ss})\left(\frac{\Theta_S}{\pi}\right)^{\frac{1}{2}} \tag{3-27}$$

(b.2) Kinetic Viscosity

Expressions for kinetic viscosity, proposed by Syamlal et al. (1993) and Gidaspow et al. (1992) are available in *FLUENT*. The expression proposed by Syamlal et al (1993) is expressed as:

$$\mu_{s,kin} = \frac{\alpha_s \rho_s d_s \sqrt{\Theta_S \pi}}{6(3 - e_{ss})}\left[1 + \frac{2}{5}\alpha_s g_{0,ss}(1 + e_{ss})(3e_{ss} - 1)\right] \tag{3-28}$$

The expression proposed by Gidaspow et al. (1992) is:

$$\mu_{s,kin} = \frac{10\rho_s d_s \sqrt{\Theta_S \pi}}{96\alpha_s(1 + e_{ss})g_{0,ss}}\left[1 + \frac{4}{5}\alpha_s g_{0,ss}(1 + e_{ss})\right]^2 \tag{3-29}$$

(b.3) Frictional Viscosity

In dense flow at low shear rate, the generation of stress is mainly due to friction between particles when the secondary volume fraction for a solid phase approaches the packing limit. Schaeffer (1987) calculated the frictional viscosity as:

$$\mu_{s,fr} = \frac{p_s \sin\varphi}{s\sqrt{I_{2D}}} \tag{3-30}$$

Where p_s is the solid pressure, ϕ is the angle of internal friction, and I_{2D} is the second invariant of the deviatoric stress tensor.

(b.4) Bulk Viscosity

The solids bulk viscosity accounts for the resistance of the granular particles to compression and expansion. It has the following form from Lun et al (1984).

$$\lambda_s = \frac{4}{3}\alpha_s\rho_s d_s g_{0,ss}(1+e_{ss})\left(\frac{\Theta_S}{\pi}\right)^{\frac{1}{2}} \tag{3-31}$$

(D) Solid-Solid Momentum Exchange Coefficient

Fluent adopts the calculation of solid-solid momentum exchange coefficient derived by Syamlal (1987). This approach is based on a simplified version of kinetic theory:

$$K_{ls} = \frac{3(1+e_{ls})\left(\frac{\pi}{2}+C_{fr,ls}\frac{\pi^2}{8}\right)\alpha_s\rho_s\alpha_l\rho_l(d_1+d_2)^2 g_{0,ls}}{2\pi(\rho_l d_l^3+\rho_s d_s^3)}|\vec{v}_l - \vec{v}_s| \tag{3-32}$$

Where e_{ls} is the coefficient of restitution, $C_{fr,ls}$ is the coefficient of friction between the l^{th} and s^{th} solid phase particle s, d_{ls} is the diameter of the particles of solid l, and $g_{0,ls}$ is the radial distribution coefficient.

(E) Granular Temperature

The granular temperature for the s^{th} solid phase is proportional to the kinetic energy of the random motion of the particles. The transport equation derived from kinetic theory is expressed as:

$$\frac{3}{2}\left[\frac{\partial}{\partial t}(\alpha_s\rho_s\Theta_S) + \nabla\cdot(\alpha_s\rho_s\vec{v}_s\Theta_S)\right] = \left(-p_s\bar{\bar{I}} + \bar{\bar{\tau}}_s\right):\nabla\vec{v}_s$$

$$+\nabla\cdot\left(k_{\Theta_S}\nabla\Theta_S\right) - \gamma\Theta_S + \varphi_{ls} \tag{3-33}$$

where $\left(-p_s\bar{\bar{I}} + \bar{\bar{\tau}}_s\right):\nabla\vec{v}_s$ is the generation of energy by the solid stress tensor,$k_{\Theta_S}\nabla\Theta_S$ is the diffusion of energy, $\gamma\Theta_S$ is the collisional dissipation of energy, and $\varphi_{ls}$is the energy exchange between the l^{th} fluid or solid phase and the s^{th} solid phase. When the Syamlal (1987) model is used, the diffusion coefficient for granular temperature is given by

$$k_{\Theta_S} = \frac{15\alpha_s\rho_s d_s\sqrt{\Theta_S\pi}}{4(41-33\eta)}\left[1 + \frac{12}{5}\eta^2(4\eta-3)\alpha_s g_{0,ss} + \frac{16}{15\pi}(41-33\eta)\eta\alpha_s g_{0,ss}\right] \tag{3-34}$$

Where

$$\eta = \frac{1}{2}(1+e_{ss}) \tag{3-35}$$

Following expression is used if the model of Gidaspow is enabled:

$$k_{\Theta_S} = \frac{150\rho_s d_s\sqrt{\Theta_S\pi}}{384(1+e_{ss})g_{0,ss}}\left[1 + \frac{6}{5}(1+e_{ss})\alpha_s g_{0,ss}\right]^2$$

$$+2\rho_s{\alpha_s}^2 d_s(1+e_{ss})g_{0,ss}\sqrt{\Theta_S/\pi} \tag{3-36}$$

The collisional dissipation of energy $\gamma\Theta_S$is represented by the expression derived by Lun et al. (1984):

$$\gamma_{\Theta_m} = \frac{12(1-{e_{ss}}^2)g_{0,ss}}{d_s\sqrt{\pi}}\rho_s{\alpha_s}^2{\Theta_S}^{3/2} \tag{3-37}$$

The transfer of the kinetic energy of random fluctuations in particle velocity from the s^{th} solid phase to the l^{th} fluid or solid phase is represented by φ_{ls}:

$$\varphi_{ls} = -3\,K_{ls}\Theta_S \tag{3-38}$$

FLUENT uses an algebraic relation for the granular temperature by neglecting convection and diffusion in the transport equation of granular temperature.

3.1.3 Turbulence Model

Three methods are provided in Fluent for modeling turbulence in multiphase flows within the context of the *k*-*ε* models including mixture turbulence model, dispersed turbulence model and turbulence model for each phase. Considering the accuracy and computational efforts, Mixture Turbulence Model is selected for the simulation in this paper. The *k* and ε equations describing this model are as follows:

$$\frac{\partial}{\partial t}(\rho_m k) + \nabla \cdot (\rho_m \vec{v}_m k) = \nabla \cdot \left(\frac{\mu_{t,m}}{\sigma_k} \nabla k\right) + G_{k,m} - \rho_m \epsilon \tag{3-39}$$

and

$$\frac{\partial}{\partial t}(\rho_m \epsilon) + \nabla \cdot (\rho_m \vec{v}_m \epsilon) = \nabla \cdot \left(\frac{\mu_{t,m}}{\sigma_\epsilon} \nabla \epsilon\right) + \frac{\epsilon}{k}(C_{1\epsilon} G_{k,m} - C_{2,\epsilon} \rho_m \epsilon) \tag{3-40}$$

Where the mixture density and velocity, ρ_m and $\vec{v}_m$ are computed from

$$\rho_m = \sum_{i=1}^{N} \alpha_i \rho_i \tag{3-41}$$

and

$$\vec{v}_m = \frac{\sum_{i=1}^{N} \alpha_i \rho_i \vec{v}_i}{\sum_{i=1}^{N} \alpha_i \rho_i} \tag{3-42}$$

the turbulent viscosity, $\mu_{t,m}$is computed from

$$\mu_{t,m} = \rho_m C_\mu \frac{k^2}{\epsilon} \tag{3-43}$$

and the production of turbulence kinetic energy, $G_{k,m}$ is computed from

$$G_{k,m} = \mu_{t,m}(\nabla \vec{v}_m + (\nabla \vec{v}_m)^T) : \nabla \vec{v}_m \tag{3-44}$$

The constants in these equations are the same as described for the single-phase *k*-*ε* model in *FLUENT*.

3.2 CFD Mathematical Model

3.2.1 Input of Oil Sand Properties for Simulation

Oil sand slurry investigated here is considered to be a transient multiphase flow of incompressible and immiscible phases including hot water, oil and solid phases. Oil and water can be combined to generate a pseudo single fluid phase that their properties are averaged into a single liquid phase. This thesis develops a Two-Phase (sand, pseudo single fluid phase combining water and bitumen) CFD model to simulate the oil sand flow behavior.

Bitumen viscosity in oil sand depends significantly on the temperature, as shown in Figure 3-2. Puttagunta (1993) developed a viscosity-temperature correlation over a wide range of temperatures for all Alberta heavy oils and bitumen. Properties of oil sand adopted from Frimpong's (2002) and Puttagunta (1993) are given in Table 3-1. Viscosity and density of the pseudo single fluid phase are obtained by averaging the properties of bitumen and water according to the principles developed by Refutas (2000), as shown in Table 3-2. Since field data are obtained for a wide range of slurry densities (specific gravities between 1.37 and 1.57). The specific gravity is acted as a variable input parameter in the CFD model. The appropriate specific gravity of 1.44 is obtained by comparing simulated pressure drop data with operational data in the field pipelines. The corresponding mass fraction of sand, water and bitumen are 50%, 40% and 10%, respectively.

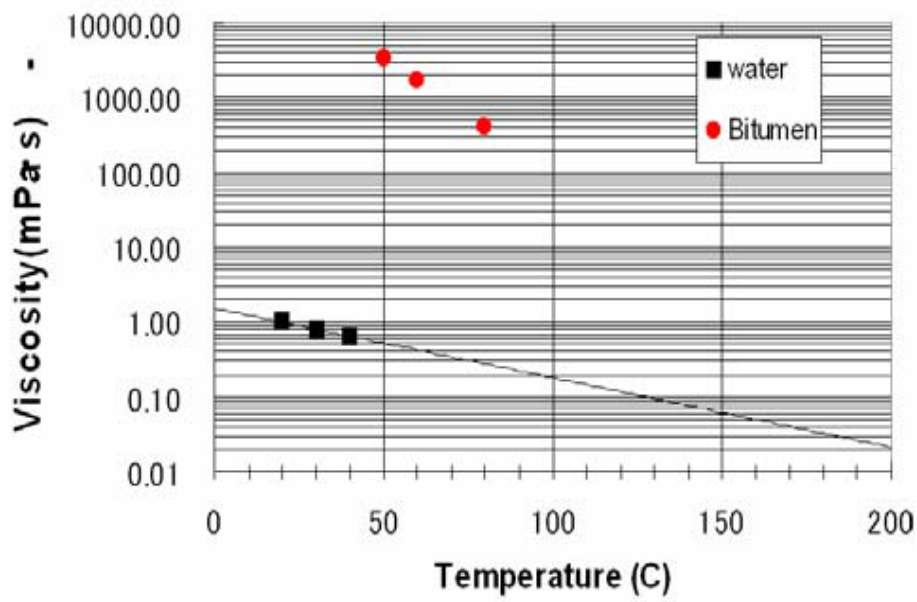

Figure 3-2 Temperature dependence of bitumen viscosity (after Mochinaga, 2006)

Table 3-1 Oil sand properties for CFD simulation

Type	parameter	Values
Phase data	Solid density	2650 kg/m^3
	Water density	1000 kg/m^3
	Bitumen density	960 kg/m^3
	Temperature	25 ℃
	Water viscosity	0.001003Pa.s
	Bitumen viscosity	30Pa.s
	Solid inlet fraction	50% (by mass)
	Water inlet fraction	40% (by mass)
	Bitumen inlet fraction	10% (by mass)

Table 3-2 Numerical solution input data of the CFD Two-Phase Model

Type	parameter	Values
Phase data	Solid density	2650 kg/m3
	Pseudo single fluid phase	990 kg/m^3
	Pseudo single fluid phase viscosity	0.007Pa.s
	Solid inlet fraction	50% (by mass)
	Pseudo single fluid phase inlet fraction	50% (by mass)

3.2.2 Mathematical Model

Fluent has several general multiphase model like the Volume of Fluid (VOF) model, mixture model and Eulerian model. The choosing of a specific multiphase flow model depends on the volume fraction of solid particles and on fulfilment of the simulation requirements. The VOF model is appropriate for stratified or free-surface flows, and the mixture and Eulerian models are appropriate for flows in which the phases mix or separate and/or dispersed-phase volume fractions exceed 10% (Fluent User Guide, 2003). As a matter of fact, solid concentration in oil sand slurry could even reach 60% that the mixture model and Eulerian model can be used. Due to the high solid concentration presented, the dispersed phases would be concentrated in portions of the pipe domain, Eulerian model therefore would be more appropriate in this case. For the two versions of the Eulerian model, the granular version is chosen since the non-granular model does not consider friction and collisions between particles. This effect is believed to be of great importance in a slurry pipeline system. Besides, a maximum packing limit can be set in the granular version, making it more suitable for modelling flows with a particulate secondary phase.

3.2.2.1 Geometry and Meshing

To conduct this study, three three-dimensional horizontal pipes are created using Ansys-Geometry. Pipes are of diameter 0.6096m, 0.7366m and 0.762m, respectively. Pipe length of 30m is used. The geometries are then imported to Fluent to simulate pressure drop. Table 3-3 lists the mesh details of all three pipes. Hexahedral mesh is used, due to its capabilities in providing high-quality solution, with a fewer number of cells than comparable tetrahedral mesh for simple geometry (Fluent User Guide, 2003). The pipe meshing details are shown in Figure 3-3 and Figure 3-4.

Table 3-3 Mesh details of all three pipes

	Number of nodes	Number of hexahedral elements
Pipe (0.6096m)	215,517	203,236
Pipe (0.7366m)	391,092	376,110
Pipe (0.762m)	291,249	275,716

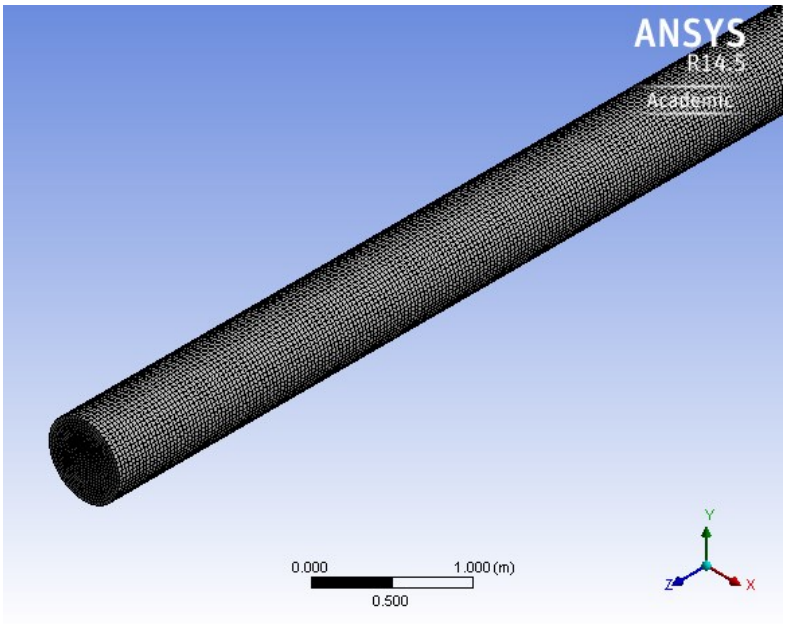

Figure 3-3 Meshing of the pipe geometry

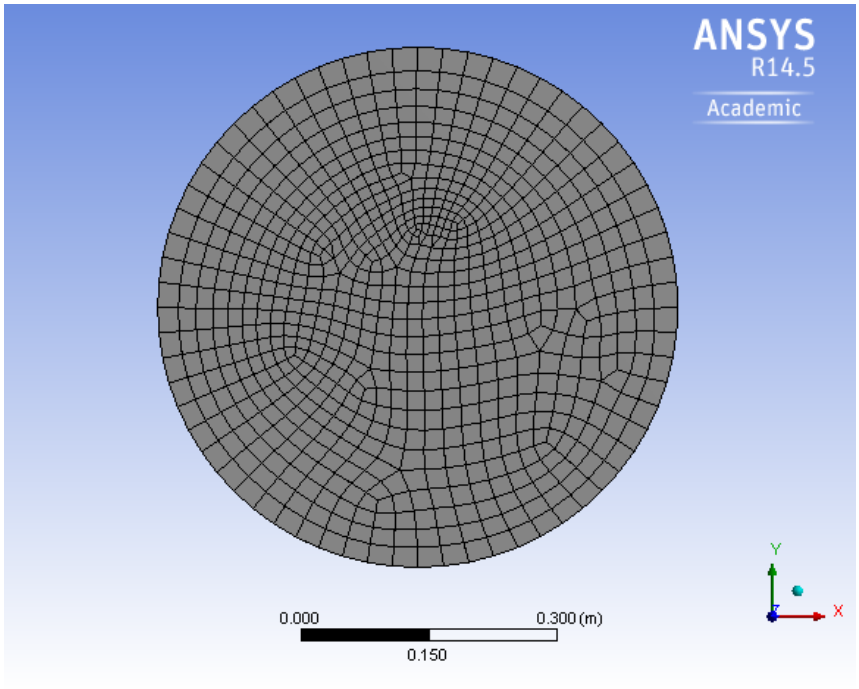

Figure 3-4 Pipe Inlet domain

3.2.2.2 Mesh Independency Study

A mesh independency study is performed using the pipe of diameter 0.6096m. Reasonable results independent of the grid size can be obtained. The results are shown in Table 3-4.

Table 3-4 Mesh independency study for the pipe (Diameter: 0.6096m, length: 30 m)

Slurry velocity	Mesh elements	Pressure drop predicted (Pa)	Error*
4 m/s	203,236	5975	2.1%
	393,296	5980	2.2%
	748,238	6019	2.9%
	2,277,056	6074	3.8%

* Experimental pressure drop for oil sand slurry in pipe of diameter 0.6096m at the velocity 4m/s is 195 *Pa/m*.

Results indicated that reasonable pressure drop independent of the size of the grid could be obtained when the grid size reaches adequately small and accurate value.

3.2.2.3 Wall Function and Boundary Layer

Turbulent flows are greatly affected by the presence of walls. The near-wall modeling significantly impacts the accuracy of numerical solutions. In the near-wall region, solution variables normally have large gradients. In addition, the momentum and other scalar transport occur most vigorously. Numerous experiments have shown that the near-wall region can be largely subdivided into three layers (Fluent User Guide, 2003). The innermost layer is called the “viscous sub-layer". Laminar flow is the primary pattern here and the (molecular) viscosity dominates the momentum, heat or mass transfer. The layer where turbulence plays a major role is called the fully-turbulent layer. The interim region exists between the viscous sub-layer and the fully turbulent layer. Effects of molecular viscosity and turbulence are equally important in this region. The subdivisions of the near-wall region are illustrated in Figure 3-5, which is plotted in semi-log coordinates. These three zones are separated based on their corresponding wall y+, namely the viscous sub-layer ($y^+<5$), buffer layer or blending region ($5<y^+<30$) and fully turbulent or log-law region ($30<y^+<60$).

Similar to local Reynolds number, the wall y+ is a non-dimensional distance used in CFD to determine how coarse or fine a mesh is for a particular flow. It is normally expressed as the ratio between the turbulent and laminar influences in a cell. Tangential velocity fluctuations are reduced by viscous damping, while the normal fluctuations are reduced by kinematic blocking at inner part of the near wall region. However, the turbulence is rapidly increased by the turbulent kinetic energy produced due to the presented large gradients in mean velocity at the outer part of the near-wall region. Values of y+ close to

the lower bound (y+≈30) are most desirable for wall functions (Fluent User Guide, 2003).

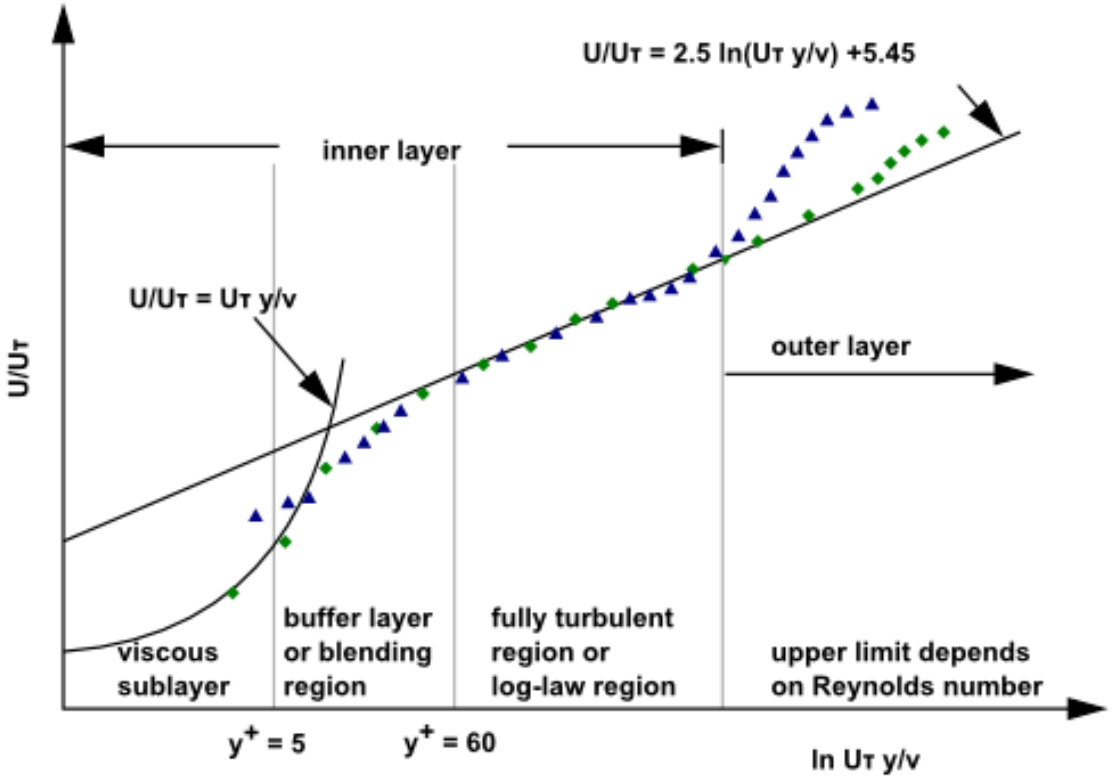

Figure 3-5 Subdivisions of the Near-wall Region (after Fluent User Guide, 2003)

Due to the large gradient presented, the fact that near-wall requires fine grids makes the calculation to become more expensive both in terms of time and the complexity of the equations. Computer of greater memory and faster processing is needed. Successful predictions of wall-bounded turbulent flows require accurate characterization of the flow in the near-wall region. The *k*-*ε* model is primarily valid for turbulent core flows where in the regions somewhat far from walls. Wall-function is developed in Fluent to make the *k*-*ε* model suitable for wall-bounded flows. A wall function is a collection of semi-empirical formulae and functions. It provides a cheaper calculation by substituting the fine grids with a set of equations linking the solutions' variables at near-wall cells and the corresponding quantities on the wall.

In this thesis, the Scalable wall function proposed by Launder and Spalding (1974) is used. Launder proposes that in the scalable wall-function approach, the viscosity affected sub-layer region is bridged by employing empirical formulas to provide near-wall boundary conditions for the mean flow and turbulence transport equations. These formulas connect the wall conditions (e.g. the wall shear stress) to the dependent variables at the near-wall grid node, which is presumed to lie in the fully-turbulent region of the boundary layer. The wall function helps in more precise calculation of near-wall shear stresses for both liquid and solid phases in the Eulerian two-phase model. A boundary layer that contains five cells with a distance of the cell adjacent to the wall at 5% of the diameter of the pipe and a growth factor of 1.2 is initially employed on the wall to improve the performance of the wall function, as shown in Figure 3-6. The y+/y* adaption function in Fluent is also adopted to fulfil the requirement of y+ for the cell adjacent to the wall. The y+ in this thesis falls between 30 and 200.

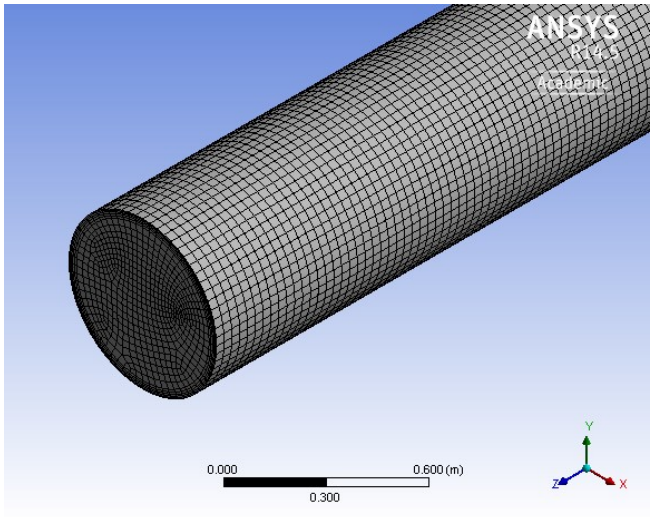

Figure 3-6 Boundary layer of the pipe

3.2.2.4 Boundary Conditions

The calculation domain is bounded by three faces including the inlet boundary, the wall boundary, and the outlet boundary. At the inlet, velocities and concentrations of liquid and solid phases are specified. The mean flow velocity is measured experimentally in field using an electromagnetic flowmeter. Velocities of the solid and liquid phases are specified as the same. Velocities of magnitudes of 3 m/s, 4 m/s and 5 m/s are used as input for the model. As mentioned above, the appropriate slurry specific gravity 1.44 is obtained by comparing simulated pressure drop data with operational data in field pipelines. The corresponding volume fractions of sand and liquid phase are 0.27 and 0.73, respectively. Detailed input parameters are shown in Table 3-5.

Table 3-5 Boundary conditions of the model

Type	Parameter	Values
Phase data	Solid density	2650 kg/m^3
	Liquid-phase density	992 kg/m^3
	Solid volume fraction	0.27
	Liquid-phase viscosity	0.007Pa.s
	Solid diameter	0.18 mm
	Velocity	3m/s, 4m/s and 5m/s

The inlet is specified as velocity-inlet; the outlet pressure is specified as atmospheric pressure. At the wall, the liquid and particles velocities are set to zero as no-slip condition.

3.2.2.5 Solution Strategy and Convergence

For the purpose of obtaining satisfactory accuracy, stability and convergence, a second-order upwind discretisation scheme is used for the momentum equation, and a first-order

upwind discretization is used for volume fraction, turbulent kinetic and turbulent dissipation rate. The convergence criterion is based on the residual value of the calculated variables including continuity, mass and velocity components, turbulent kinetic energies, turbulent dissipation energies and volume fraction. Threshold values are set to 1e-04 of the initial residual value of each variable. Phase-coupled Simple algorithm is used in pressure–velocity coupling. The calculation also applies other solution strategies like the reduction of under-relaxation factors of momentum, volume fraction, turbulence kinetic energy and turbulence dissipation for better convergence and stability. A time step of 0.0001s is initially set up and gradually increased during the simulation for the transient calculation.

3.3 Simulation Results of the Eulerian Two-Phase Model

3.3.1 Velocity Profile

Three velocity magnitudes of 3 m/s, 4 m/s and 5 m/s are used as input for the model. The liquid phase velocity profile (slurry velocity: 4 m/s) in the horizontal pipe of diameter 0.6096m is shown in Figure 3-7. Velocity profiles in horizontal slurry flow are directly linked to many factors including the solid concentration, particle size and mixture viscosity. It can be seen that the velocity profiles are mostly symmetrical about the pipe axis. The maximum local velocity 4.581 m/s is found in a little bit upper portion of the pipe and not at the centerline. The sand deposition at the bottom of the pipe may impede the velocity development in the lower portion of the pipe.

As fluid progresses from the inlet to outlet, flow develops gradually to a fully turbulent flow. The velocity profile development of oil sand slurry from the inlet to outlet is indicated in Figure 3-8. Contour plots of liquid velocity along the pipe cross section at various axial positions separated by 10 m intervals are indicated. Significant differences

in liquid velocity can be observed between the inlet and outlet axial positions. Generally, the velocity contour plots are mostly symmetrical about the pipe axis.

Velocity profile indicates the similar pattern in pipes of diameter 0.7366m and 0.762m. However, solid particle size is specified as the median size of 0.18 mm in this thesis, the effects of particle size distribution and large particle on velocity profile are not indicated from the simulation. Kalekudithi (2009) predicted liquid velocity profiles for slurries containing particles with different sizes (90, 270 and 480μm, respectively). His study showed that the velocity profiles became increasingly asymmetrical with increasing particle size. This phenomenon has also been demonstrated experimentally by Gillies (2004) and Roco (1983).

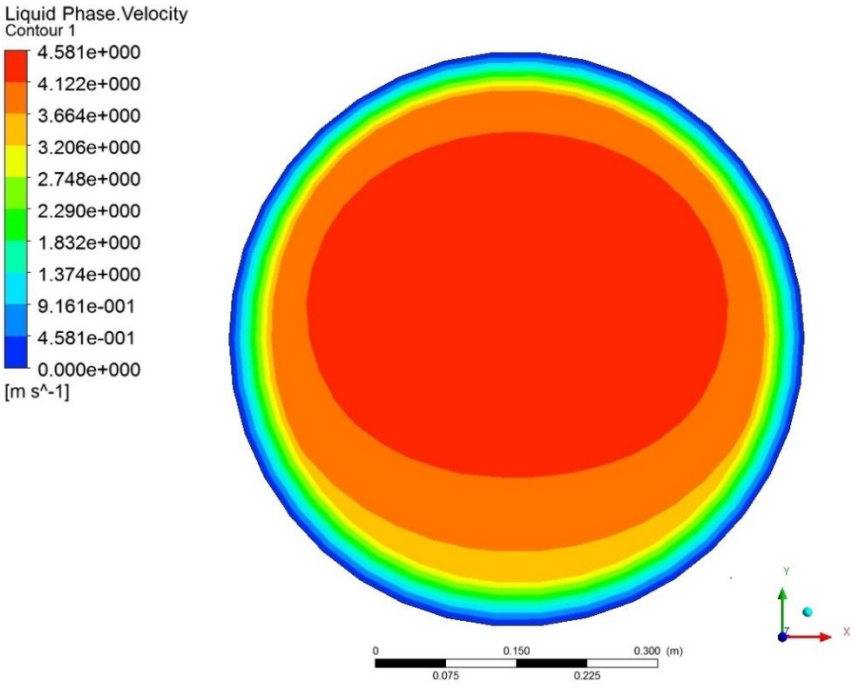

Figure 3-7 Liquid phase velocity profile at the outlet along the pipe of diameter 0.6096m (velocity: 4m/s)

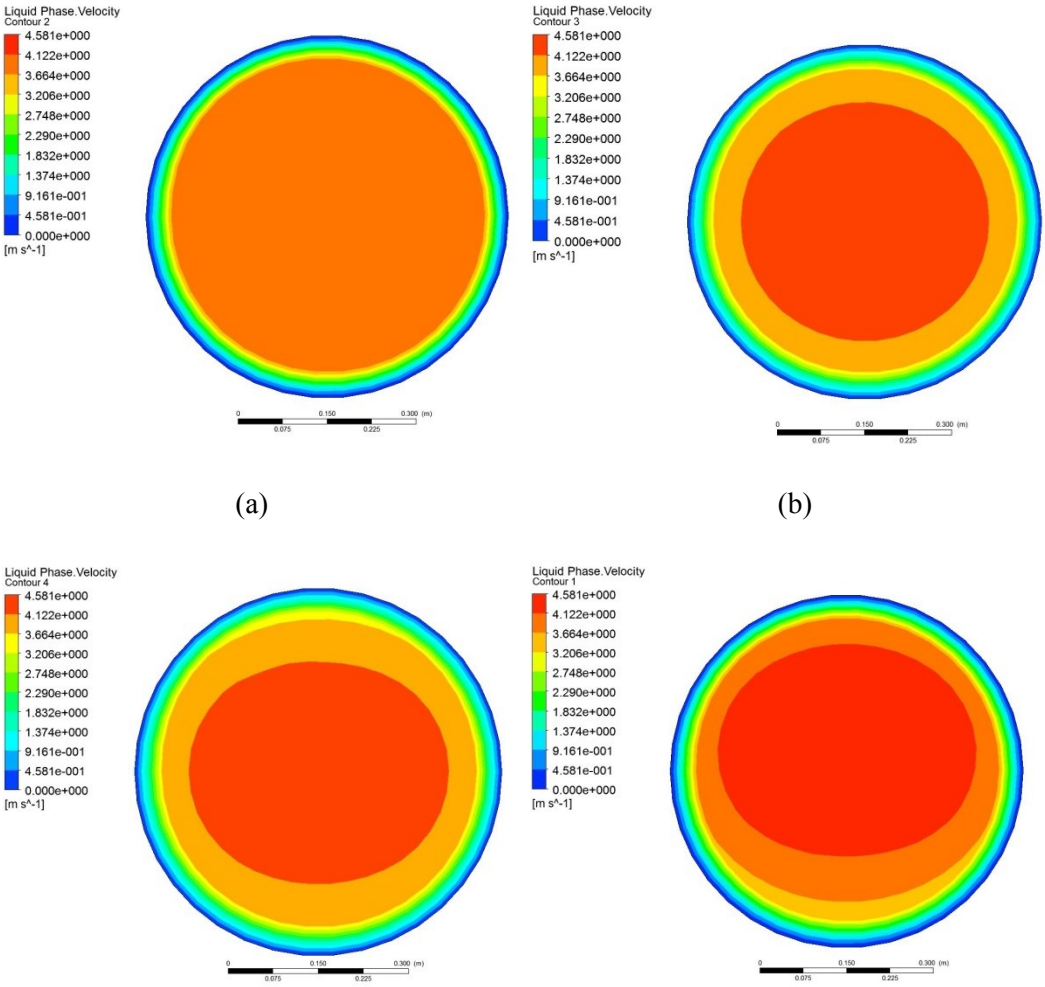

Figure 3-8 Liquid phase velocity development along the pipe of diameter 0.6096m (velocity: 4m/s) a) Inlet; (b) z = 10 m (axial coordinate); (c) z = 20 m (axial coordinate); (d) Outlet

3.3.2 Sand Concentration Profile

Sand concentration profile is influenced by many parameters including mixture velocity, mixture density, pipe diameter, particle size, and particle density. Due to the high concentration presented of up to 50% by mass, the ability of a model to predict the solid concentration distribution profiles remains great significance. In addition, the evaluation or prediction of pipeline wear also demands the knowledge of solids distribution across

the pipe cross-section (Guangchuan, 2013). Reasonable velocity should be ensured to suspend solid particles in the pipe. Figure 3-9 shows the predicted concentration profiles (slurry velocity: 4m/s) at the outlet in the pipe of diameter 0.6096m. The maximum sand volume concentration of 0.3137 is found at the bottom of the pipe. Figure 3-10 indicates the contour plots of sand concentration along the pipe cross section at various axial positions. It can be observed from that for these high concentration slurries, fluid turbulence is not fully effective in suspending the solid particles and sand gradually deposits along the pipe from the inlet to outlet. The nearly identical contour plots shown in Figure 3-10 for axial positions (e) and (f) shows that the obtained numerical results are basically provided for fully developed flow. Sand concentration profile indicates the similar pattern in pipes of diameter 0.7366m and 0.762m.

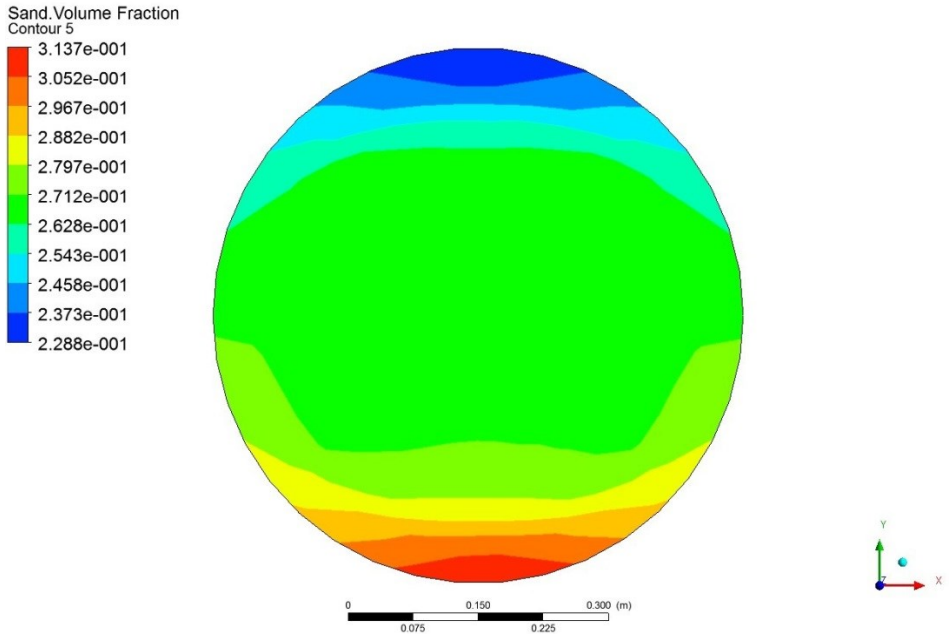

Figure 3-9 sand concentration profile at the outlet along the pipe of diameter 0.6096m (velocity: 4m/s)

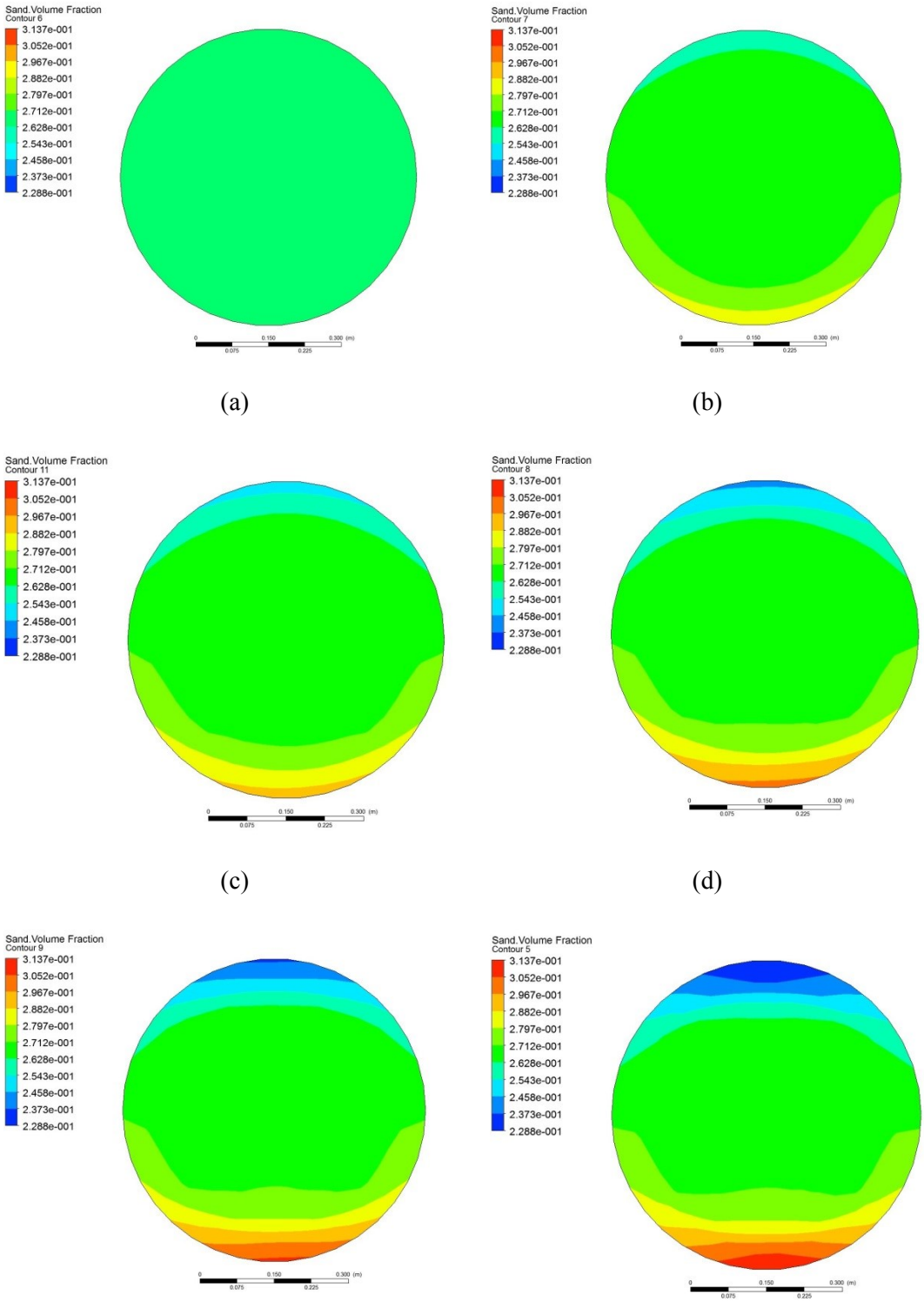

Figure 3-10 Sand concentration profile development along the pipe of diameter 0.6096m

a) Inlet; (b) z = 10 m; (c) z = 15 m; (d) z = 20 m; (e) z = 25m; f) Outlet

3.3.3 Pressure Drop

3.3.3.1 Analysis of Field Pipeline Performance

For the operation of sand slurry pipelines in the oil sand industry, presence of lumps, stationary bed formed and hydrodynamic roughness all contribute to slurry pressure drops measured in industrial pipelines. The focus of this thesis for oil sand slurry pressure drop is intended to be general that pipelines selected here represent the most important hydrotransport applications in the oil sand industry and are not identified by the name of the owner. Most of these Pipelines are from Suncor Energy Inc. and Syncrude Canada Ltd. Data is monitored continuously and recorded in digital form. Operating data are obtained for a wide range of slurry densities (specific gravities between 1.37 and 1.57) and ore grades under different velocities. These samples selected are estimated to adequately represent a range of operating conditions but should not be regarded as limiting cases. Oil sand hydrotransport pipelines of diameter 0.6096m, 0.7366m and 0.762m are considered here. Pressure drop data of these pipelines under different slurry velocities is obtained. The data is shown in Figure 3-11.

The quotient of the pressure difference and the density is calculated for a 30-minute average period. Operators examine the 30-minute averages of the flow rate, density and static pressure data to identify periods in which the flow rate and density are nearly constant. There is no kinetic energy difference over the pipe section since the pipe cross-sectional area is constant. The Mechanical Energy Balance between the upstream plane1 and downstream plane 2 is interpreted as:

$$(P_2 - P_1) + \rho g(h_2 - h_1) + \rho g j L = 0 \tag{3-45}$$

Where P is the water static pressure, ρ is the density, j is the friction loss per pipe length and L is pipe section length. This equation indicates that the frictional pressure loss ($\rho g\, j$

L) is obtained by subtracting the gravitational effect ρg ($h_2 - h_1$) from the total pressure drop ($P_1 - P_2$).

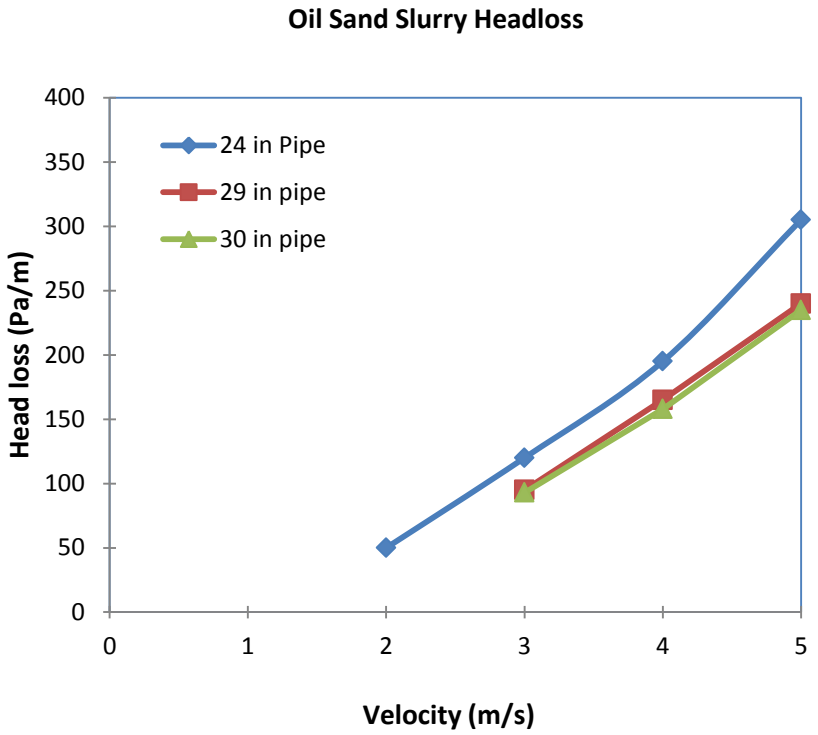

Figure 3-11 The average friction pressure losses for oil sand slurry flow in Pipelines of diameter 0.6096m, 0.7366m and 0.762m under different velocities.

Concept of reasonable hydrodynamic roughness should be taken into consideration in respect to pressure drop. A new steel pipe will typically have a roughness of 45 μm. A pipe with a coarse particle, oil sand slurry flowing would have a roughness of 3-8 μm. (Shook, 2002). Slurries containing bitumen, which is normally seen in oil sand industry, would result in increased hydrodynamic roughness to 500 μm or even higher. The thickness of a bitumen coating on the wall depends on bitumen concentration, slurry velocity plus temperature. Increased temperature or velocity would help to decrease the bitumen wall thickness. The hydrodynamic roughness of the pipe walls can be greater than expected if the walls are coated with bitumen, or less if the walls have been

smoothed from abrasion by sand (Sanders, 2000). In addition to the hydrodynamic wall roughness, presence of lumps or large particles, as mentioned in Chapter 2, is expected to contribute to greater slurry pressure drop measurements than those predicted by the model. Due to these uncertainties, pipe simulated in *Fluent* is assumed to be smooth with its roughness being zero. Since operating data are obtained for a wide range of slurry densities (specific gravities between 1.37 and 1.57), slurry density is acted as a variable parameter in the CFD model. The appropriate slurry density is obtained by comparing simulated pressure drop data with operational data in field pipelines. The mathematical model developed suitable to modelling oil sand slurry flow in horizontal pipeline then will be used in the AFSS folding pipelines.

Pressure drops along the pipe at different velocities for the pipes of diameters 0.6096m, 0.7366m and 0.762m are shown in Figure 3-12, Figure 3-13 and Figure 3-14, respectively.

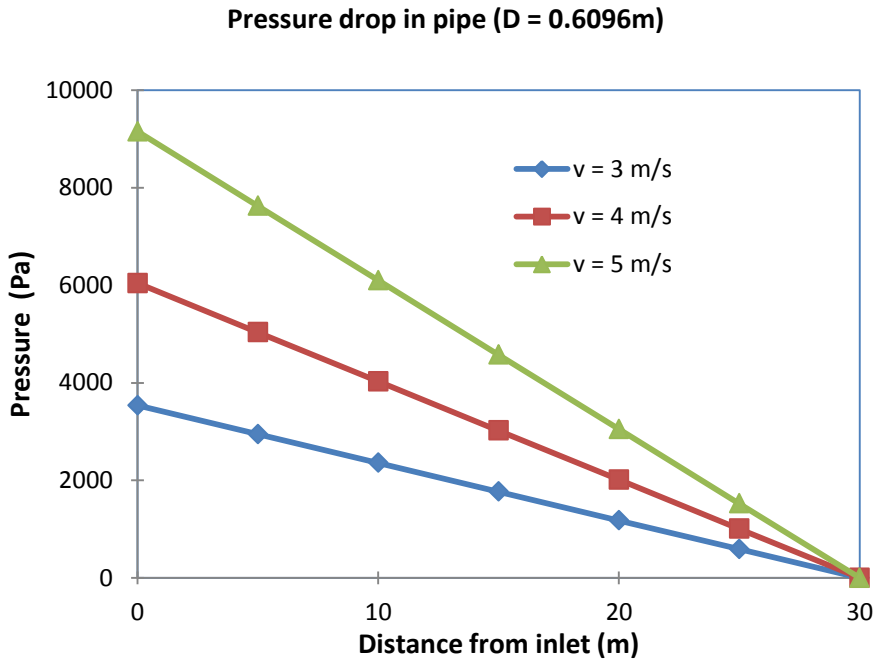

Figure 3-12 Pressure drop along the pipe of diameter 0.6096m at different velocities

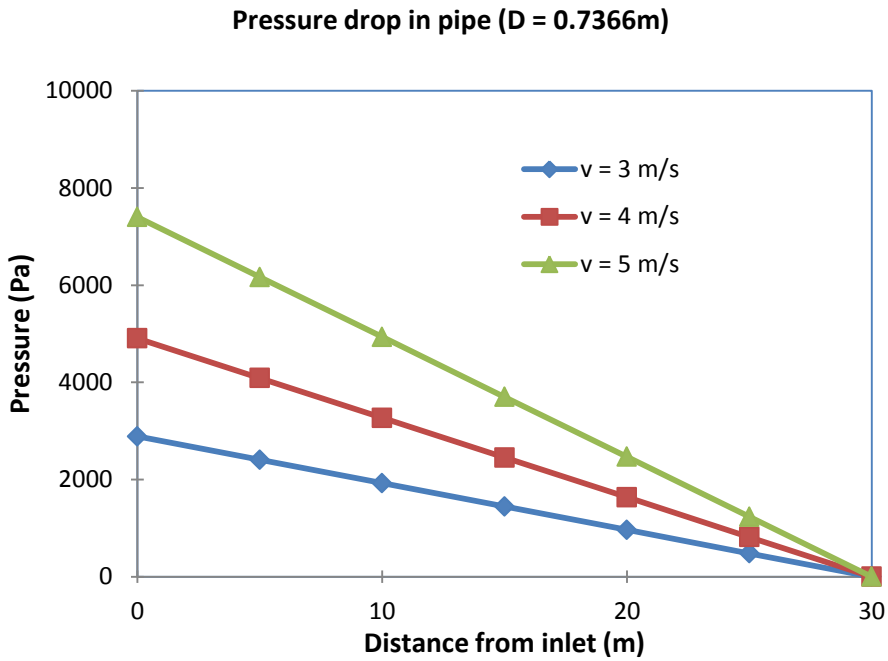

Figure 3-13 Pressure drop along the pipe of diameter 0.7366m at different velocities

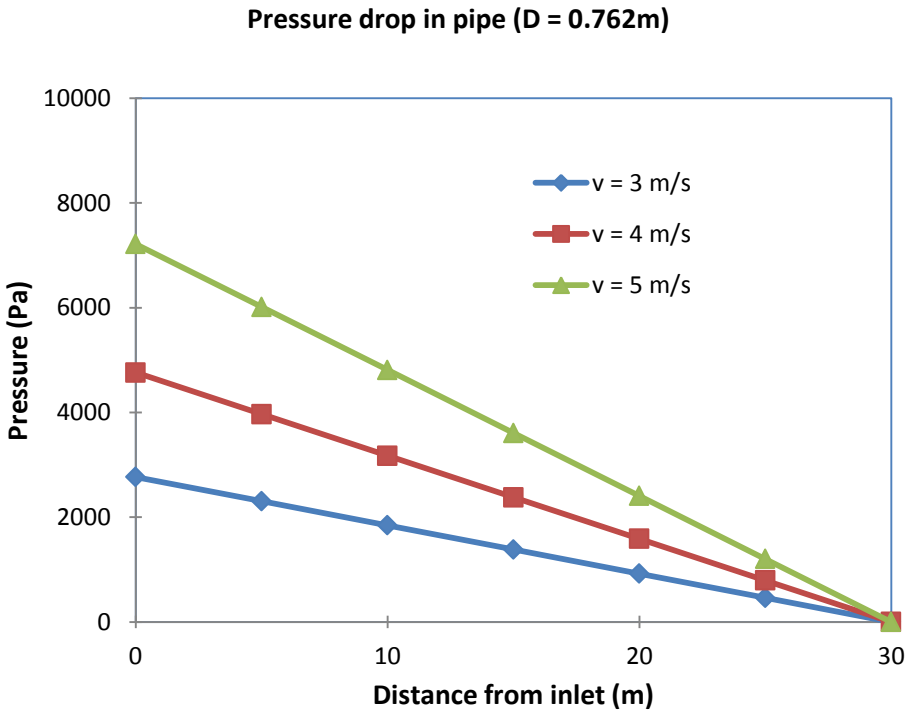

Figure 3-14 Pressure drop along the pipe of diameter 0.762m at different velocities

The comparison between operational and predicted pressure drop data at different velocities for the pipes with diameters 0.6096m, 0.7366m and 0.762m are shown in Figure 3-15, Figure 3-16 and Figure 3-17, respectively. The predicted pressure drop is in good agreement (within a percentage deviation of $\pm 3\%$) with the experimental measurements for the wide range of slurry flow conditions.

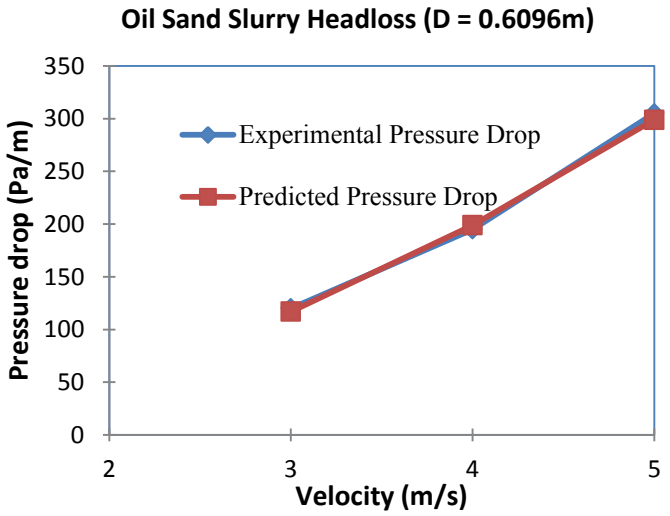

Figure 3-15 Comparison between operational and predicted pressure drop in pipe of diameter 0.6096 m

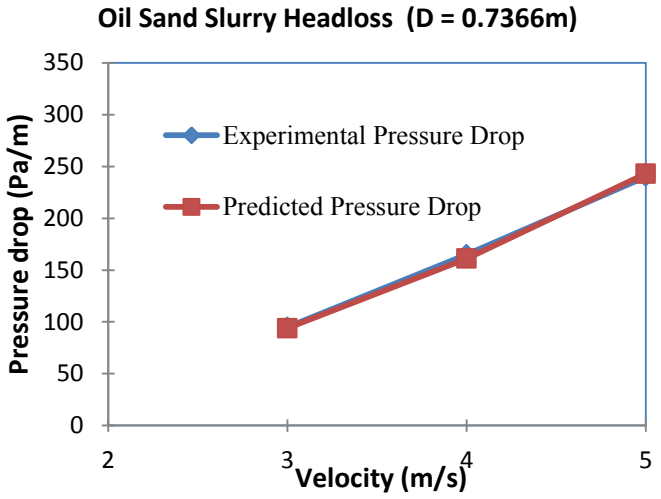

Figure 3-16 Comparison between operational and predicted pressure drop in pipe of diameter 0.7366 m

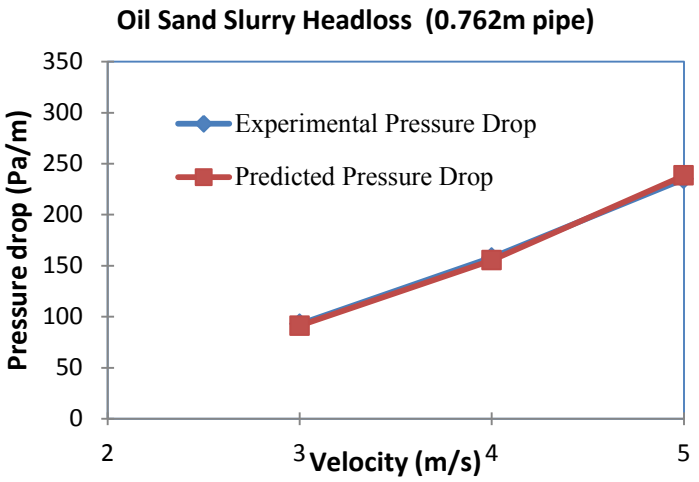

Figure 3-17 Comparison between operational and predicted pressure drop in pipe of diameter 0.762m

The Eulerian Multiphase model has accurately predicted the pressure drop of oil sand slurry flow in horizontal pipeline. The same mathematical model will be used to predict the pressure drop in the folding pipelines of the At Face Slurry System, which will be introduced in the following section.

4 At Face Slurry Experiment

4.1 Set Up of Experimental Pipe Loop

Figure 4-1 shows the At Face Slurry Test loop. The test loop is 27.5 m long of inside diameter 50.8 mm. it is built to obtain hydraulic data regarding various characteristics of the flow including flow rates, pressure drop and flow patterns across the pipe cross-section, etc.

Figure 4-1 At face slurry test loop

The rig consists of a closed circulating pipe loop, slurry mixture tank and a centrifugal pump to maintain the slurry flow. Water and the solid particles are mixed mechanically in the tank. A stirring arrangement is provided to keep the slurry well mixed. An electromagnetic flux flowmeter is installed in the pipe for continuous monitoring of slurry velocity. Since it is a closed loop, water and solid particles pumped into the pipe system are accurately measured to ensure the desired slurry solid concentration. Each experiment is repeated three times to obtain the average value for accuracy demand. For

the study in this thesis, sand concentration of 10%, 25% and 50% (by mass) are used under the velocity of 2.3 m/s. The detailed velocity selection (above the slurry deposition velocity) of the experimental system is described in section 4.2.

To measure the pressure drop distribution in the pipe and the swivel joint unit, pressure transducers are provided at the inlet of the loop, upstream and downstream sides of each swivel bend. Detailed distribution of the pressure transducers in the swivel joint units are shown in Figure 4-2.

Figure 4-2 Pressure transducer location

The swivel joint unit is made up of two commercial bends with r/d of 1.5 and a vertical pipe section. The bend is capable to swivel around the vertical axis of the vertical pipe section so that the pipes could fold and extend to make zigzag movements and display different configurations. Transparent pipes are used to connect these swivel joint units for the convenience to observe the flow pattern and sand deposition of the slurry. The solid

particles used here is silica sand. These solid particles have a measured specific gravity of 2.65 and a median particle size of 480μm. For the two-phase flow, an equivalent pipe length to pipe diameter ratio of approximately 100–150 is required for fully developed flow (Mazumder, 2008). Due to limitations of the experimental test system, the ratio used in this study is 30. Experimental loop is checked for correct alignment between the bend and the straight pipe before taking each measurement. The pipe loop experiments are conducted with different alignment angles of 0 degree, 30 degree, 60 degree and 80 degree, respectively. These configurations are shown in Figure 4-3 to Figure 4-6.

Figure 4-3 Pipe loop with alignment angle 0^o

Figure 4-4 Pipe loop with alignment angle 30^o

Figure 4-5 Pipe loop with alignment angle 60^{o}

Figure 4-6 Pipe loop with alignment angle 80^{o}

4.2 Slurry Velocity Requirement for the Experiment

The minimum velocity required to suspend a solid particle in a pipe is known as the limit-deposit velocity, V_L. It is also referred to as the deposition velocity, which corresponds to the velocity for transition from the moving bed regime to the heterogeneous regime. Durand (1953) conducted extensive tests with pipes ranging in diameter from 38 to 710 mm, using particles of sand and gravel measuring from 0.2 to 25 mm, at volume concentrations between 2 and 23%. Figure 4-7 shown below summarizes Durand's work for solid particles of uniform or nearly uniform size and for particles of rather non-uniform size distribution. V_L therefore can be determined from this figure that once the particle diameter *ds*, pipe diameter *D*, solid specific gravity *S*, solid volumetric

concentration *Cv*, and gravitational acceleration *g* are known. The value of *ds* is based on the mesh size that passes 85% for non-uniform particles. The equation to obtain V_1 is expressed as,

$$F_1 = \frac{V_1}{\sqrt{2gD(S-1)}} \tag{4-1}$$

Where F_1 is the densimetric Froude number of the slurry flow in pipe corresponding to particle deposition, F_L can be determined from Figure 4-7.

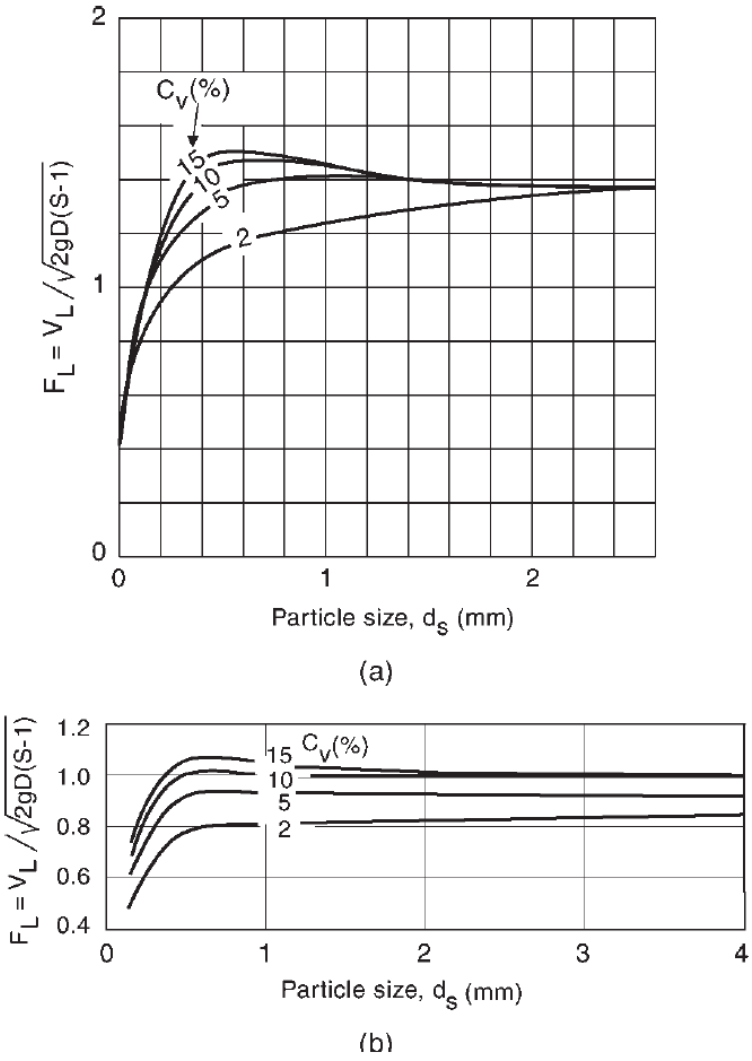

Figure 4-7 limit-deposit velocity for solid particles: (a) uniform size particles; (b) non-uniform size particles (after Durand, 1953)

A velocity V slightly higher than V_L (say $V = 1.2\ V_L$) would be necessary to make sure that the flow is heterogeneous with fully suspended solids. The other deposition velocity theory is proposed by Govier (1972). The velocity demanded for hydrautransport is rather greater than the velocity required to keep the solids "float" in an upward stream of the fluid. Normally, a useful practice guide for choosing the velocity is

$$v = K\sqrt{\left[d\left(\frac{s-r}{r}\right)\right]} \tag{4-2}$$

Where K is a constant, equal to 3 or 4, depending on the particle size, d is the pipe diameter in metres, s is the solid density and r is the fluid density.

The experiment in this thesis investigates the pressure drop of slurry with sand concentration 0.04, 0.12 and 0.27 (by volume) in a flexible pipe loop of diameter 0.0508m. According to the equations above, take the maximum F_L value of 1.2, the velocity required to transport the slurry should be above 1.87 m/s. In this experiment, velocity of 2.3 m/s is used based on the pump power provided.

4.3 CFD Simulation of the Experimental Pipe Loop

4.3.1 Geometry

To conduct this study, four three-dimensional pipes with alignment angles of 0^o, 30^o, 60^o and 80^o are created using Ansys-Geometry. Pipes are of diameter 0.0508m. The entire pipe length simulated is 6.095m. The geometries are then imported to Fluent to simulate pressure drop. Table 4-1 lists the mesh details of all the four pipes. Hexahedral mesh is mainly used, due to its capabilities in providing high-quality solution. The bend in the unit is refined by using the function Face Sizing. The geometries with different configurations are shown in Figure 4-8. Each unit includes two swivel joint units and three horizontal pipe sections.

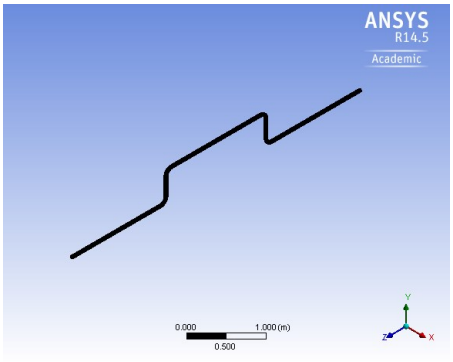

(a) Alignment angle 0^o

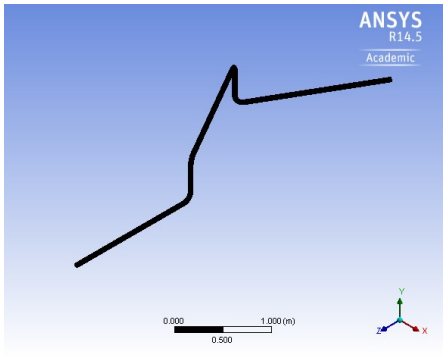

(b) Alignment angle 30^o

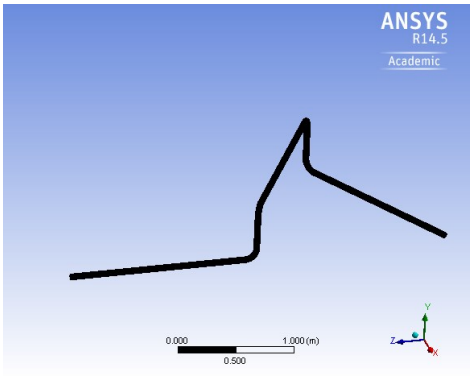

(c) Alignment angle 60^o

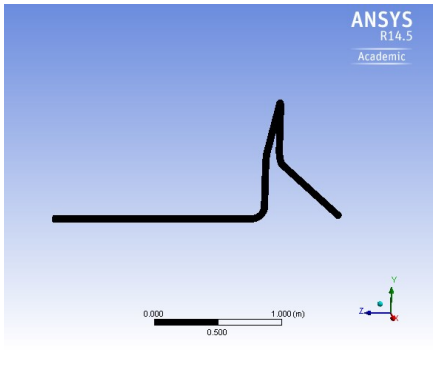

(d) Alignment angle 80^o

Figure 4-8 Pipe geometries with different alignment angles

Table 4-1 Mesh details of all four pipes with different configurations

	Number of nodes	Number of hexahedral elements
Pipe (0^o)	413,285	390,524
Pipe (30^o)	406,868	382,800
Pipe (60^o)	414,794	389,400
Pipe (80^o)	442,535	417,120

4.3.2 Boundary Conditions

The calculation domain is bounded by three faces including the inlet boundary, the wall boundary, and the outlet boundary. At the inlet, velocities and concentrations of liquid

and solid phases are specified. Velocities of the solid and liquid phases are specified as the same. Velocity of magnitude of 2.3 m/s is used. Sand concentration of 0.04, 0.12 and 0.27 (by volume) are investigated. Detailed input parameters are shown in Table 4-2.

Table 4-2 Boundary conditions of the model

Type	Parameter	Values
Phase data	Sand density	2650 kg/m^3
	Water density	1000 kg/m^3
	Sand volume fraction	0.04, 0.12 or 0.27
	Water viscosity	0.001003 Pa.s
	Sand diameter	0.48 mm
	Velocity	2.3 m/s

The inlet is specified as velocity-inlet; the outlet pressure is specified as atmospheric pressure. At the wall, the liquid and particles velocities are set to zero as no-slip condition. The solution strategy and convergence are the same as the model developed for horizontal pipe in Chapter 3.

4.4 Results and Analysis

4.4.1 Velocity and Concentration Profile

Since the velocity and concentration profiles in the swivel joint unit present mostly similar pattern for all the experiments, the concentration and velocity profiles of the slurry with sand concentration (*Cv = 0.12*) and alignment angle 0^o are illustrated. The velocity profiles in the two swivel joints are shown in Figure 4-9 and Figure 4-10, respectively.

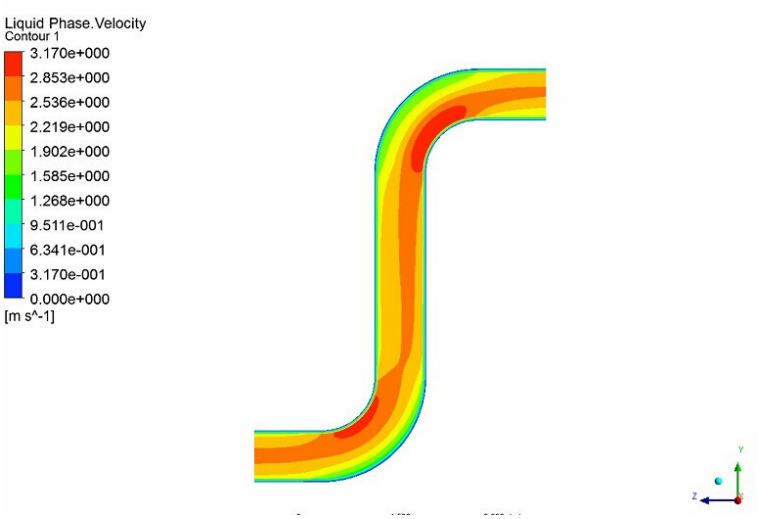

Figure 4-9 Velocity profile in the first swivel joint unit (*Cv =0.12*, alignment angle *0*^{o})

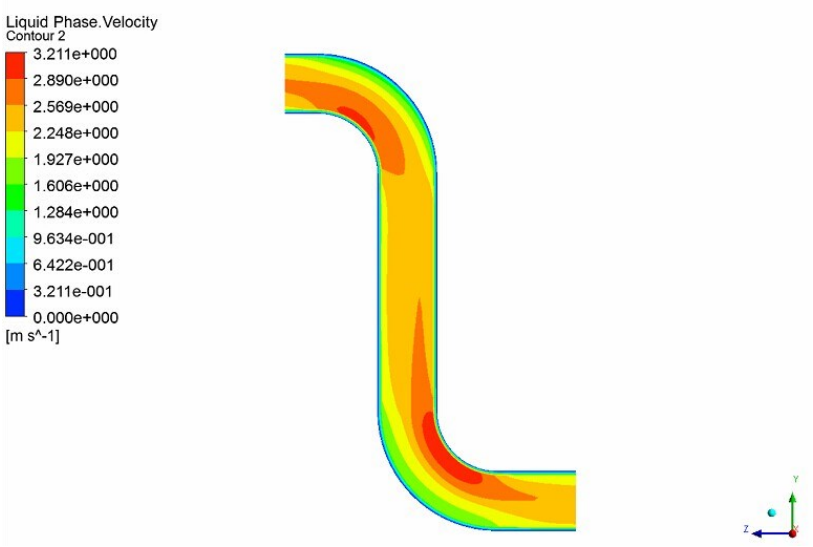

Figure 4-10 Velocity profile in the second swivel joint unit (*Cv =0.12*, alignment angle *0*^{o})

These two figures depict that a lower velocity magnitude exists close to the outer radius and a higher velocity near the inner radius. At the inner radius, recirculation of fluid is suspected, contributing a good percentage of the pressure drop in the bend. On the straight run of the elbow downstream, a reversed picture emerges with the higher

velocities at the outer radius and the lower ones close to the inner radius due to larger centrifugal forces on the outside radius.

As indicated in Figure 4-11 and Figure 4-12, it can be observed that for these high concentration slurries, fluid turbulence is not fully effective in suspending the solid particles and sand gradually deposits along the pipe from the inlet to outlet. Maximum sand volume fraction of up to 0.194 (when Cv = 0.12) is found at the outer edge of the bend from horizontal to vertical upward direction and at the inner edge of the bend from horizontal to vertical downward direction.

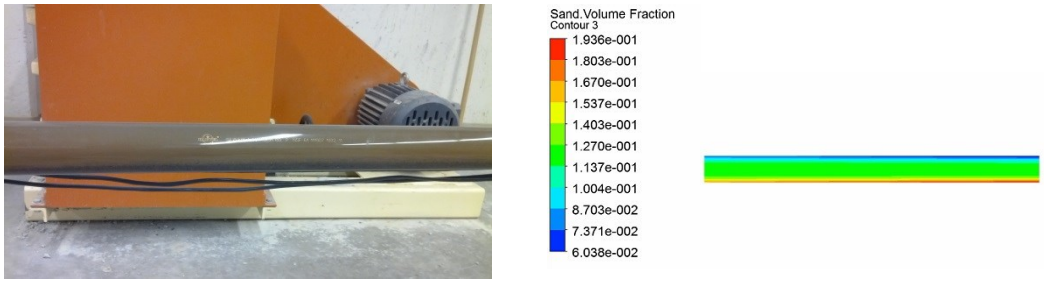

(a) (b)

Figure 4-11 Sand deposition in the (a) transparent experimental pipe; (b) corresponding pipe section in CFD simulation

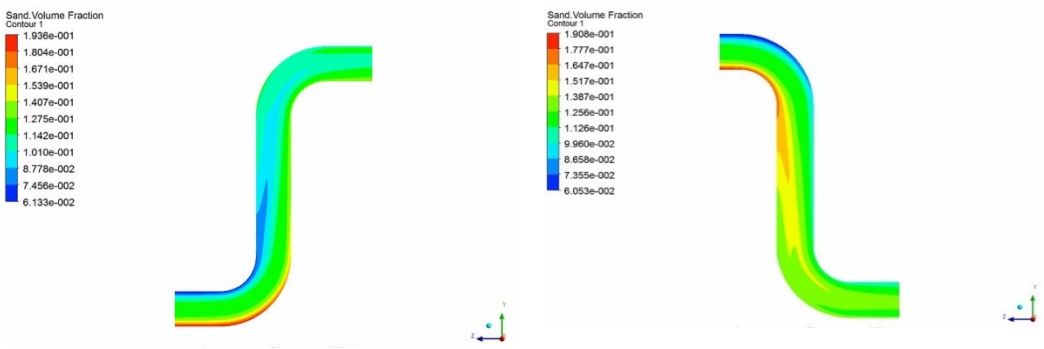

Figure 4-12 Sand concentration profiles in the two swivel joint units (Cv =0.12, alignment angle 0^o)

4.4.2 Pressure Drop Profile

Pressure drops at loop inlet, swivel joint unit and outlet are measured experimentally. Experimental data are compared to the results modelled by running the commercial CFD package Fluent. Predicted and experimental pressure drops of sand slurry with different sand volume fractions under alignment angle 0^{o} are shown in Figure 4-13, Figure 4-14 and Figure 4-15.

Bend and swivel joints have a significant impact on the pressure drop. As shown in these figures, the pressure steadily decreases along the flow, the gap in the graph indicate the pressure decreases rapidly in comparison with the horizontal pipeline as the flow approaches the pipe bend. Due to the influence of gravity, the first gap is much higher than the second gap in the graph.

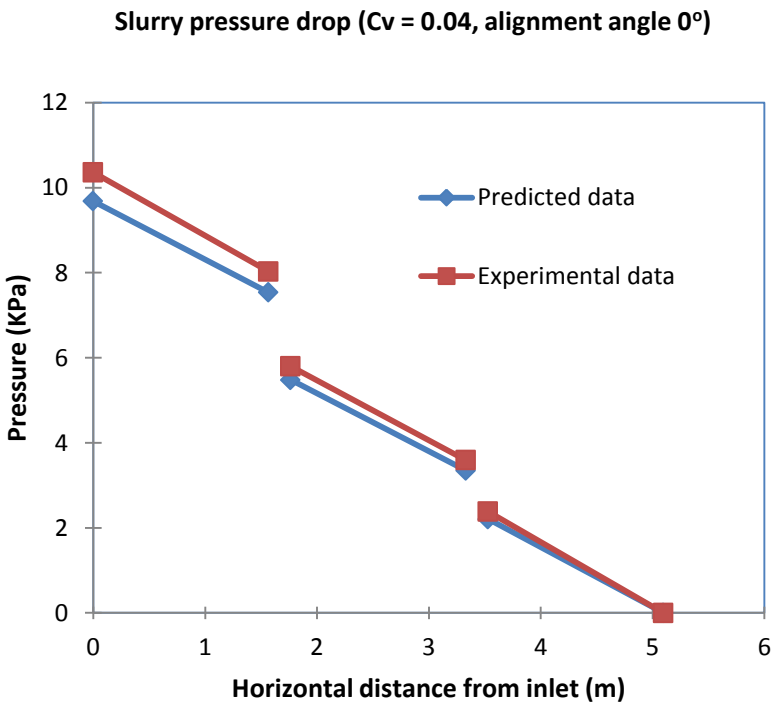

Figure 4-13 Pressure drop of sand slurry (Cv = 0.04, alignment angle 0^{o})

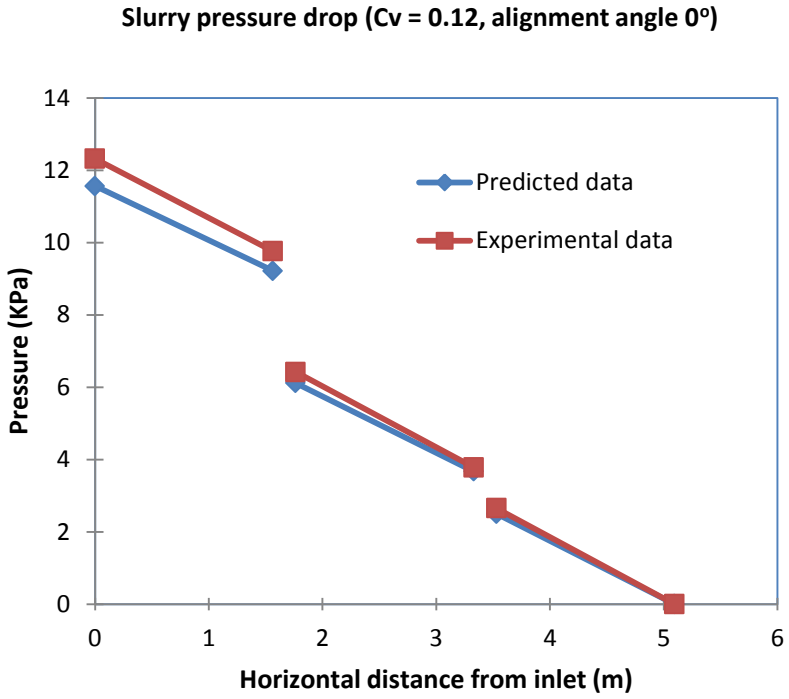

Figure 4-14 Pressure drop of sand slurry (Cv = 0.12, alignment angle 0°)

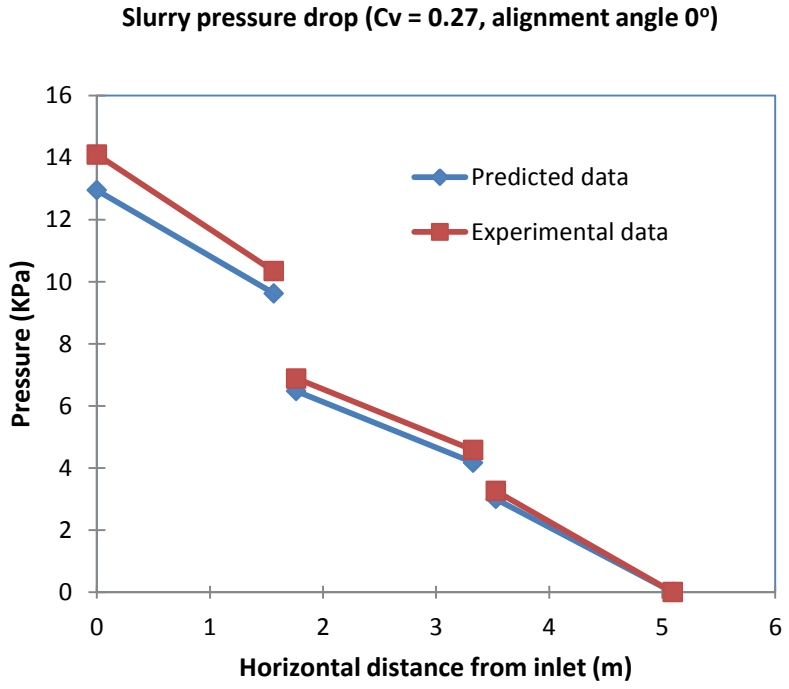

Figure 4-15 Pressure drop of sand slurry (Cv = 0.27, alignment angle 0°)

The centrifugal force acting on the fluid produces a radial pressure gradient when flow through the bend. A double spiral flow field is created by the fluid at the center of the pipe moving towards the outer edge and coming back along the wall towards the inner edge because of the radial pressure gradient. The change in the direction of flow results in flow separation and causes pressure losses by both friction and momentum exchanges. The overall pressure drop gap is equal to the sum of pressure drop resulted from friction in a straight pipe of equivalent length depending mainly on the Reynolds number and friction losses resulted from change of direction depending mainly on the curvature ratio and the bend angle.

Predicted and experimental pressure drop data of at face slurry loop unit under different alignment angles is shown in Table 4-3. Detailed comparisons are shown in Figure 4-16 and Figure 4-17. Pressure drop in the Table is obtained by dividing the pressure drop from inlet to outlet by the entire length of the flow path (straight pipe section) of the simulated at face slurry loop.

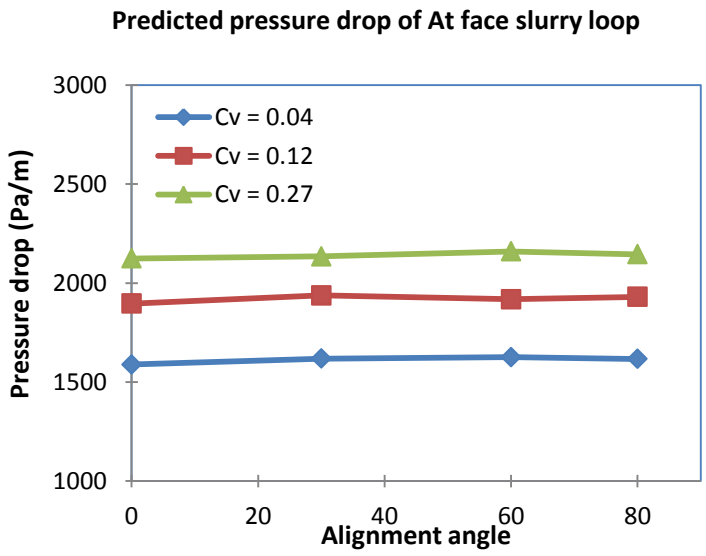

Figure 4-16 Predicted pressure drop of at face slurry loop unit under different alignment angles

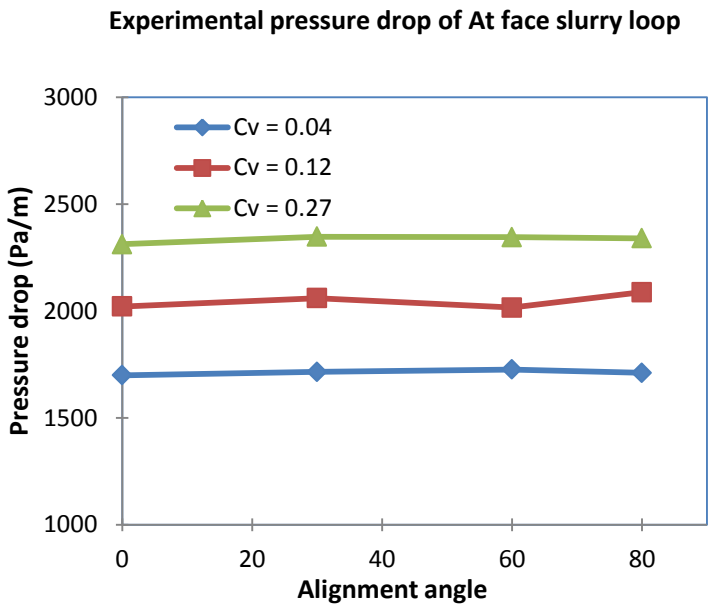

Figure 4-17 Experimental pressure drop of at face slurry loop unit under different alignment angles

Table 4-3 Predicted and experimental pressure drop data of at face slurry loop unit

Cv (alignment angle)	Pressure Drop (Pa/m)	
—	Experimental	Predicted (Error)
0.04 (0^o)	1699 Pa/m	1588 Pa/m (-6.5%)
0.04 (30^o)	1715 Pa/m	1618 Pa/m (-5.7%)
0.04 (60^o)	1726 Pa/m	1625 Pa/m (-5.9%)
0.04 (80^o)	1710 Pa/m	1616 Pa/m (-5.5%)
0.12 (0^o)	2021 Pa/m	1896Pa/m (-6.2%)
0.12 (30^o)	2060 Pa/m	1937 Pa/m (-6.0%)
0.12 (60^o)	2016 Pa/m	1918 Pa/m (-4.9%)
0.12 (80^o)	2088 Pa/m	1930 Pa/m (-7.6%)
0.27 (0^o)	2312 Pa/m	2079 Pa/m (-10.1%)

0.27 (30^o)	2347 Pa/m	2134 Pa/m (-9.1%)
0.27 (60^o)	2345 Pa/m	2159 Pa/m (-8.0%)
0.27 (80^o)	2320 Pa/m	2135 Pa/m (-8.0%)

The At Face Slurry System consists of a flexible arrangement of pipelines that are capable to fold and extend to display any alignment angle. Results in Figure 4-16 and Figure 4-17 indicate that the impact of alignment angle is not very influential. Pressure drop is more related with the change of direction in the bend. The results indicate that the Eulerian Multiphase model is reasonably effective in predicting the pressure drop of the at face slurry loop (with a percentage error in the range $\pm 10\%$) at all the efflux concentrations and configurations considered in this experiment. The Eulerian Multiphase model underestimates the pressure drop compared to experimental data. The deviation may result from the input parameter of solid particle size. The Eulerian model requires the input of median particle size and doesn't consider the effect of size distribution on pressure drop. As mentioned previously, the presence of large particles, or lumps, is expected to produce slurry pressure drop measurements that are greater than those predicted by the model. A model to predict friction losses for slurries containing large particles should be developed.

5 CFD Simulation of At Face Slurry System

5.1 Geometry

To conduct this study, four three-dimensional pipes with alignment angles of 0^o, 30^o, 60^o and 80^o are created using Ansys-Geometry. Pipes are of diameter 0.762m. The single geometry includes two swivel joint units and three horizontal pipe sections. The entire straight pipe length is 156.0452m. The configurations are the same as shown in Figure 4-8. Table 5-1 lists the mesh details of all the four pipes. Hexahedral mesh is mainly used, and the bend in the unit is refined by using the function Face Sizing.

Table 5-1 Mesh details of all four pipes with different configurations

	Number of nodes	Number of hexahedral elements
Pipe (0^o)	794,328	768,675
Pipe (30^o)	787,372	742,675
Pipe (60^o)	8032,46	778,672
Pipe (80^o)	858,046	813,276

5.2 Boundary Conditions

As the same introduced in simulating the experimental at face slurry loop, the calculation domain is bounded by three faces including the inlet boundary, the wall boundary, and the outlet boundary. Velocities of the solid and liquid phases are specified as the same at the inlet. Parameters of oil sand properties obtained in the CFD simulation of horizontal pipe in Chapter 3 are applied here. Velocity of 4 m/s and sand concentration of 0.27 (by volume) are used. Detailed input parameters are shown in Table 5-2.

Table 5-2 Input parameters of the model

Type	Parameter	Values
Phase data	Sand density	2650 kg/m^3
	Liquid-phase density	992 kg/m^3
	Sand volume fraction	0.27
	Liquid-phase viscosity	0.007 Pa.s
	Sand diameter	0.18 mm
	Velocity	4.0 m/s

The solution strategy and convergence are the same as the model developed for horizontal pipe in Chapter 3.

5.3 Results

5.3.1 Velocity and Concentration profile

Velocity and concentration profiles under the alignment angle 0^o are shown in Figure 5-1, Figure 5-2 and Figure 5-3.

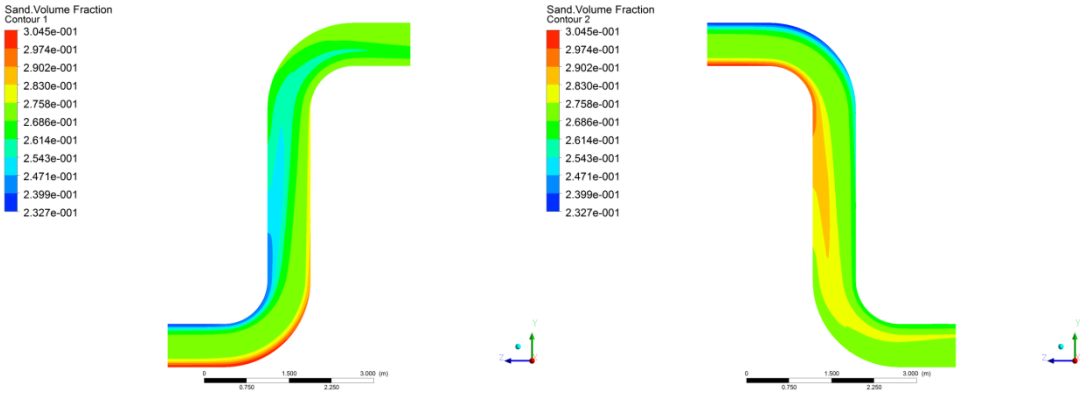

Figure 5-1 Sand concentration profiles in the two swivel joint units (*Cv* =0.27, alignment angle 0^o)

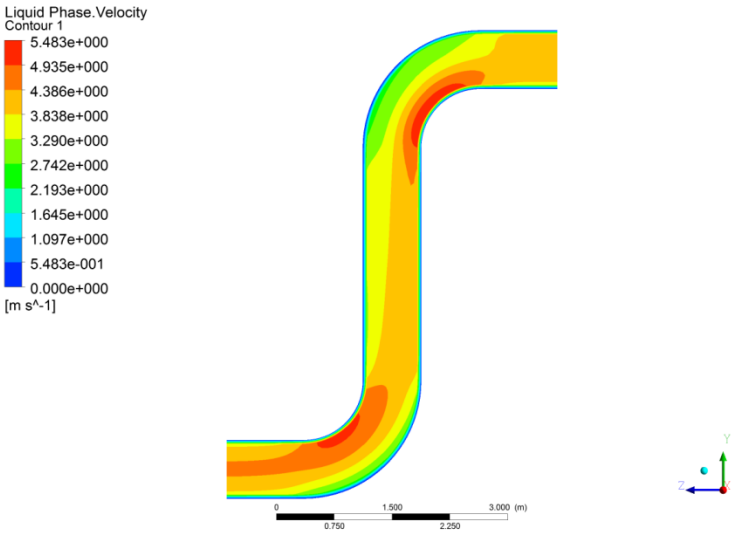

Figure 5-2 Velocity profile in the first swivel joint unit (*Cv* =0.27, alignment angle 0^{o})

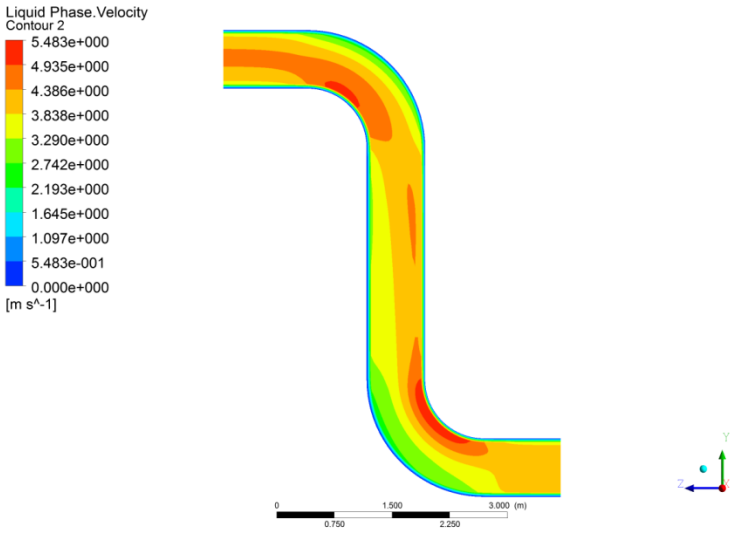

Figure 5-3 Velocity profile in the second swivel joint unit (*Cv* =0.27, alignment angle 0^{o})

They indicate the similar patterns as shown in the experimental at face slurry loop mentioned in Chapter 4. The maximum velocity and minimum velocity are found at the inner edge and outer edge of the bend in the swivel joint unit respectively. The maximum sand volume fraction is 0.3045 found at the entrance of each swivel joint unit.

5.3.2 Pressure Drop

The pressure drop data is shown in Table 5-3. Pressure drops for oil sand slurry flow with solid volume fraction of 0.27 at mean flow velocity of 4.0 m/s under different alignment angles of 0^o, 30^o, 60^o and 80^o are simulated. Each AFSS unit includes two straight folding pipelines and two swivel joint units, as shown in Figure 1-2.

Table 5-3 Predicted pressure drop in one typical unit of the at face slurry system

Cv (alignment angle)	Predicted Pressure Drop (Pa)
0.27 (0^o)	23377
0.27 (30^o)	23595
0.27 (60^o)	23329
0.27 (80^o)	23215

The whole AFSS consists of five typical units. The folding pipelines have a retracted length of approximately 80m and extended length of 500m (length of each straight folding pipeline is 50m). The swivel joint unit consists of two elbows and a vertical pipe section of 3.0226 m.

Since the pipe cross-sectional area is constant, there is no kinetic energy difference over the pipe section The Mechanical Energy Balance between the upstream plane1 and downstream plane 2 is interpreted as the same as equation (3-45):

$$(P_2 - P_1) + \rho g(h_2 - h_1) + \rho g j L = 0 \tag{5-1}$$

Where P is the mixture static pressure, ρ is the density, j is the friction loss per pipe length and L is pipe section length. This equation indicates that the frictional pressure loss

($\rho g\ j\ L$) is obtained by subtracting the gravitational effect ρg ($h_2 - h_1$) from the total pressure drop ($P_1 - P_2$).

The pipe length L in the equation represents the straight pipe length only and does not include the flow distance through the elbows. It is technically wrong and a waste of time trying to measure all the flow path lengths, the error is normally well within the tolerance of the results (Crane, 1991). For a typical at face slurry system unit, the whole straight pipe length equals to 106.0452m (two folding pipelines of length 100m and two vertical pipe sections in swivel joint units of length 6.0452m). So the pressure gradient can be obtained as shown in Table 5-4.

Table 5-4 Predicted pressure gradient in one typical unit of the at face slurry system

Cv (alignment angle)	Predicted Pressure Gradient (Pa/m)
0.27 (0^o)	220
0.27 (30^o)	222
0.27 (60^o)	220
0.27 (80^o)	219

As described in Chapter 3, the pressure gradient of oil sand slurry flow in horizontal pipe with the same solid volume fraction of 0.27 and velocity of 4 m/s is 158 Pa/m. Compared to the stationary pipeline, more powerful pump are required for the feasibility of the at face slurry system. The at face slurry design will allow the pipes to make zigzag movements and follow the shovels as needed at mining face. Results in Table 5-4 indicate that alignment angle displayed has no obvious impact on the pressure drop.

6 Conclusion

6.1 Conclusion

The At Face Slurry System introduces a unique set of hydraulic transport problems. This thesis focuses to develop the mathematic models governing the friction loss associated with the AFSS. The oil sand slurry flow is simulated using the academic CFD package Fluent. Results are compared to field pressure drop data from oil sand industry for the stationary pipeline system. A flexible arrangement of pipe loop imitating the AFSS is set up in the laboratory. Experimental and modelling results are obtained and compared to test the accuracy of CFD modelling to predict pressure drop in flexible pipeline system. Based on these work, oil sand flow in the flexible pipeline of AFSS is simulated to validate its technical viability. Summarily, some conclusions through this study can be reached as follows:

1. The granular Eulerian Multiphase model has accurately predicted the pressure drop of oil sand slurry flow in horizontal pipeline. The predicted pressure drop is in good agreement (within a percentage deviation of $\pm 3\%$) with the experimental measurements for the wide range of slurry flow conditions (specific gravities between 1.37 and 1.57). For a typical slurry (specific gravity 1.44, $Cv = 0.27$, d = 0.18 mm and V = 4 m/s) in the pipe of diameter 0.762m, the experimental and simulated pressure drop are 158 Pa/m and 155 Pa/m, respectively.

   .

2. Results from the experimental at face slurry loop indicate that a lower velocity magnitude exists close to the outer radius and a higher velocity near the inner radius at the elbows of the swivel joint unit. For high concentration slurries, fluid turbulence is not fully effective in suspending the solid particles and sand

gradually deposits along the pipe from the inlet to outlet. Pressure decreases rapidly in comparison with the horizontal pipe as the flow approaches the elbow in the swivel joint unit. Eulerian multiphase model is reasonably effective in predicting the pressure drop of the at face slurry loop (with a percentage error in the range $\pm 10\%$) at all the efflux concentrations and configurations considered in this experiment. The model underestimates the pressure drop compared to experimental data. Presence of large particles, or lumps, is expected to produce slurry pressure drop measurements that are greater than those predicted by the model.

3. The simulated pressure drop for a typical oil sand slurry (specific gravity 1.44, Cv = 0.27, d = 0.18 mm and V = 4 m/s) in a single unit of the AFSS of diameter 0.762m is 220 Pa/m. This alternative haulage system requires more powerful pump to satisfy its capability to create slurrified minerals from the mining faces to be transported to the processing plant.

4. The at face slurry design allow the pipes to make zigzag movements and follow the shovels as needed at mining face. Results indicate that alignment angle displayed has no obvious impact on the pressure drop.

6.2 Recommendations

To make the AFSS a viable technology to meet the challenges in oil sands mining operations in a sustainable environment, the research in the AFSS will be demanded in the following areas:

1. The cause of difference between the experimental and predicted friction losses in the at face slurry loop should be investigated. A model to predict friction losses for slurries containing large particles should be developed.

2. Scale effect between the experimental pipe loop set up in the lab and large industrial pipe utilized in the At Face Slurry System remains further investigation.

3. Oil sand is a three-phase system that it contains water, sand and bitumen. The thesis only conducted experimentation of sand slurry flow in the at face slurry loop. Oil sand three-phase flow in the experimental at face slurry pipe loop should be conducted in the future.

7 Bibliography

Aekula, S. F. (2009). CFD predictions and experimental comparisons of pressure drop effects of turning vanes in 90 degree duct elbows. *Journal of Energy Engineering*, vol. 135, no. 4, pp. 119-126.

Akilli, H. L. (2001). Gas-solid flow behavior in a horizontal pipe after a 90° vertical-to-horizontal elbow. *Powder Technol.*, 116 (1), 43–52.

Alves, G. E. (1954). Co-current liquid-gas flow in a pipe-line contactor. *Chemical Engineering Progress*, vol. 50, no. 9, pp.449–456.

ANSYS Inc., CFX 5.6 User Manual. (2003).

Babcock and Wilcox Company. (1978). Steam: Its Generation and Use.

Chisholm, D. (1983). Two-Phase Flow in Pipelines and Heat Exchangers. *Godwin*.

Crane, C. (1991). Flow of Fluids Through Valves, Fittings and Pipe. *Tech Paper 410, 1991*.

Coffield, R. D. (1997). Irrecoverable pressure loss coefficients for two elbows in series with various orientation angles and separation distances. *ASME, Fluids Eng. Div. (Publ.) FED, 5, Fluid Measurements and Instrumentation, 7p*.

Dean, W. (1928). Fluid motion in a curved channel. *Proc. R. Soc.(Lond.) A.*, (pp. 121, 402–420).

Deobold, T. L. (1962). An experimental investigation of two-phase pressure losses in pipe elbows. *Tech. Rep.HW-SA, 2564, MSc. University of Idaho, Chemical Engineering*.

Deshmukh, S. F. (2006). Three-Dimensional CFD Predications and Experimental Comparison of Pressure Drop of Some Common Pipe Fittings in Turbulent Flow. *J. Energy Eng.*, 132:61-66.

Doron, P., & Barnea, D. (1993). A Three-Layer Model for Solid-Liquid Flow in Horizontal Pipes. *Int. J. Multiphase Flow*, 19, 1029–1043.

Doron, P., Granica, D., & Barnea, D. (1987). Slurry Flow in Horizontal Pipes-Experimental and Modeling. *Int. J. Multiphase Flow*, 13, 535–547.

Durand, R. (1953). Basic Relationships of the Transportation of Solids in pipes: Experimental Research. *Proceedings of the 5th Congress, International Association of Hydraulic Research.* Minneapolis, Minnesota.

Durand, R. (1953). Basic Solids in Pipes—Experimental Research. *Proceedings International Hydraulics Conference*, (pp. 89-103). Minneapolis, MN.

Ellison, T. K. (1997). Computational fluid dynamics CFD model for phase separation at branching tee junctions. *Proc., SPE Annual Western Regional Meeting, A New Dawn in the Old West*, (pp. 211-225).

Fitzsimmons, P. E. (1964). Two phase pressure drop in pipe components. *Tech. Rep.HW-80970 Rev 1, General Electric Research*.

FLUENT Inc., Fluent User Guide. 6.3 (February 2003). Chapter 10 Modelling Turbulence; Chapter 18 Introduction to Modeling Multiphase Flow; Chapter 20 General Multiphase Models.

Friedel, A. A. (2005). Two-phase upward flow 90◦ bend pressure loss model. *Forschung im Ingenieurwesen*, vol. 69, no. 2, pp. 120–130.

Frimpong, S. (2003). Oil sands slurry and waste recycling mechanics in. *Resources, Conservation and Recycling 39*, 33-50.

Frimpong, S. A. (2004). Oil sands slurry flow in flexible pipe. *ASME J. Fluids Eng*, 126, 133–138.

Frimpong, S., Ayodele, O. R., Awuah-Offei, K., & Brown, a. O. (2010). Numerical Simulation Software for Oil Sand Slurry Flow in Flexible Pipelines. *J. Energy Eng*, 136:50-57.

Gambill, W. (1959). How to estimate mixtures viscosities. *Chemical Engineering*, vol 66, pp 151-152.

Gidaspow, D. B. (1992). Hydrodynamics of Circulating Fluidized Beds, Kinetic Theory Approach. In Fluidization VII. *Proceedings of the 7th Engineering Foundation Conference on Fluidization*, (pp. 75-82).

Gillies, R. a. (2000). Modelling High Concentration Slurry Flows. *Can. J. Chem. Eng*, 78, 709-716.

Gillies, R. G., Shook, C. A., & Xu, J. (2004). Modelling Heterogeneous Slurry Flows at High Velocities. *Can. J. Chem. Eng*, 82, 1060–1065.

Govier, G. a. (1972). The Flow of Complex Mixture in Pipes . *Van Nostrand Reinhold.* New York.

H.Mazumder, Q. (2012). CFD Analysis of the Effect of Elbow Radius on Pressure Drop in Multiphase Flow. *Modelling and Simulation in Engineering*.

Hatziavramidis, D. S. (1997). Gas-liquid flow through horizontal tees of branching and impacting type. *AIChE J.*, 43 (7), 1675–1683.

Idelchik, I. E. (1986). *Handbook of Hydraulic Resistance.* Hemisphere Publishing Corp., Washington.

Ito, M. (1959). Friction factors for turbulent fow in curved pipes. *Trans. ASME, J. Basic Engng*, 81D, 123–134.

Cole J. S. (2004). Friction factors in two phase horizontal pipe flow. *International Communications in Heat and Mass Transfer*, vol. 31, no. 7, pp. 909–917.

Sekoda, K. (1969). Horizontal two-phase air-water flow characteristics in the disturbed region due to a 90-degree bend . *Japan Society Mechanical Engineering*, vol, 35, no. 289, pp. 2227–2333.

Kalekudithi Ekambara, R. S. (2009). Hydrodynamic Simulation of Horizontal Slurry Pipeline Flow Using ANSYS-CFX. *Ind. Eng. Chem. Res*, 48, 8159–8171.

Kaushal, D. R., & Tomita, Y. (2003). Comparative Study of Pressure Drop in Multisized Particulate Slurry Flow through Pipe and Rectangular Duct. *Int. J. Multiphase Flow*, 29, 1473–1487.

Kongkiatwanitch, S. W. (2001). Interfacial friction factor in vertical upward gas-liquid annular two-phase flow. *International Communications in Heat and Mass Transfer*, Vol 28, no. 3, pp. 323–336.

Kundu, P. a. (2002). *Fluid Mechanics, second edition.* Academic Press,.

Kutateladze, S. S. (1969). Problems of Heat Transfer and Hydraulics of Two-Phase Media. *Pergamon Press, Oxford, UK.*

Lun, G. (2004). Incorporating Matlab and fluent in an introductory computational fluid dynamics course. *Computers in Education J.*, 14 (1), 82–91.

Launder BE, S. B. (1974). The numerical computation of turbulent flows.

Lun, C. K. (1984). Kinetic Theories for Granular Flow: Inelastic Particles in Couette Flow and Slightly Inelastic Particles in a General Flow Field . *J. Fluid Mech* , vol. 140, p.223-256.

Maples., R. (2000). Petroleum Refinery Process Economics. PennWell, ISBN 978-0-87814-779-3.

Martin, J. M. (1955). Turbulent two-phase flow. *Petroleum Refiner*, vol. 34, no. 10, pp. 151–155.

Martinelli, R. W. (1949). Proposed correlation of data for isothermal two-phase two-component flow in pipes. *Chemical Engineering Progress*, vol. 45, no. 1, pp. 39–48.

McDonell, B. (2002). Slurry systems: Design and equipment selection with examples from Syncrude's operation. *Proc., MIN E 420 Seminar*.

McKee, W. (1988). An overview of the Syncrude Oilsands Mine. *The 9th Annual General Meeting of CIM.* Edmonton, Alberta.

Mochinaga, H. (2006). Properties of Oil sands and Bitumen in Athabasca. *CSPG-CSEG-CWLS Convention.*

Mori, Y., & Nakayama, W. (1967). Study of forced convective heat transfer in curved pipes 2nd Report: turbulent region. *Int. J. Heat Mass Transfer*, 10, 37–59.

Crawford, N.M. (2003). Prediction of pressure drop for turbulent fluid flow in 90 degree bend. *J. Process Mechanical Engineering*.

Noda, K. T. (1972). Studies on three-phase flow in an inclined pipe: determination of entrance region of pipe measurements of pressure loss. *Proceedings of the 2nd International Conference on Hydraulic Transport of Solids in Pipes*, (pp. 49-61). Warwick, UK.

Oroskar, A. R., & Turian, R. M. (1980). The Critical Velocity in Pipeline Flow of Slurries. *AIChE J*, 26, 551–558.

Osman, S. M. (1964). The mechanics of soil cutting blades. *Journal of Agriculture Engineering Research*, 313-328.

Spedding P.L. (2006). Prediction of pressure drop in multiphase horizontal pipe flow. *International Communications in Heat and Mass Transfer*, vol. 33, no.1053–1062.

Peniguel, C. S. M. (2003). Presentation of a numerical 3D approach to tackle thermal striping in a PWR nuclear T-junction. *ASME J. Pressure Vessel Technol.,*, 469, 125-132.

Peshkin, M. A. (1961). About the hydraulic resistance of pipe bends to the flow of gas-liquid mixtures. *Teploenergetika*, vol. 8, no.6, pp. 79–80.

Sanders, R. (2004 , August). Performance of Sand Slurry Pipelines in the Oil. *The Canadian Journal of Chemical Engineering*, 850-857.

Randall G. Gillies, C. A. (2004). Modelling Heterogeneous Slurry Flows at High Velocities. *The Canadian Journal of Chemical Engineering*, 82, 1060-1065.

Riffat, S. B. (1997). CFD prediction of k-factors of duct elbows. *Int. J. Energy Res.*, 21 (7), 675–681.

Roco, M. C., & Shook, C. A. (1983). Modeling of Slurry Flow: The Effect of Particle Size. *Can. J. Chem. Eng.*, 61, 494–503.

Rowe, M. (1970). Measurement and computation of flow in pipe bends. *J. Fluid Mech*, 43, 771-783.

Benbella, S. (2009). Gas-liquid pressure drop in vertical internally wavy 90 degree bend. *Experimental Thermal and Fluid Science*, vol. 33, no. 2, pp.340-347.

Sanchez, S. F. (2010). Pressure drop models evaluation for two-phase flow in 90 degree horizontal elbows. *Ingenieria Mecanica Techilogia Y Desarrollo*, vol. 3, no. 4, pp. 115–122.

Sanders, R. A. (2000). Bitumen Effects on Pipeline Hydraulics During Oil Sand Hydrotransport. *Can. J. Chem. Eng*, 78, 731–742.

Schaeffer, D. G. (1987). Instability in the Evolution Equations Describing Incompressible Granular Flow. J. Di . Eq. vol. 66, p.19-50.

Shook, C. A., & Daniel, S. M. (1968). Flow of Suspensions of Solids in Pipelines, Part 2: Two Mechanisms of Particle Suspension. *Can. J. Chem.Eng.*, 46, 238-244.

Shook, C. A., & Daniel, S. M. (1969). A Variable Density Model of the Pipeline Flow of Suspensions. *Can. J. Chem. Eng*, 47,196.

Shook, C. R. (2002). Pipeline Hydrotransport with Applications in the Oil Sand Industry. *Saskatchewan Research Council, Saskatoon, Canada*.

Song, X. W. (2004). Computational fluid dynamics study of the fourth generation prototype of a continuous flow ventricular assist device . *ASME J. Biomech. Eng.*, 126 (2), 180–187.

Puttagunta, V. R. (June 1993). Correlation of Bitumen Viscosity with Temperature and Pressure. *The Canadian Journal Of Chemical Engineering*, Vol, 71.

Wallis, G. B. (1969). One Dimensional Two-Phase Flow, McGraw-Hill.

Wang, J. A. (2001). A CFD-based correlation for mass transfer coefficient in elbows. *Int. J. Heat Mass Transfer*, 44 （9）， 1817–1822. .

Wasp, E. J. (1970). Deposition Velocities, Transition Velocities and Spatial Distribution of Solids in Slurry Pipelines. *Proceedings of the 1st International Conference on the Hydraulic Transport of Solids in Pipes (Hydrotransport 1),BHRA: Fluid Engineering*, (pp. 53-76). Cranfield, U.K.

Wilson, K. (1976). A Unified Physically Based Analysis of Solid-Liquid pipeline Flows. *Proc. 4th Int. Conf. On Hydraulic Transport of SolidsH.S.Stephens, Ed., BHRA Fluid Engineering, Cranfi eld, UK*, (pp. Paper A1, pp. 1–16).

Wilson, K. A. (September, 2000). Near-Wall Fluid Lift of Particles in Slurry Pipelines. *Proc. 10th Int. Conf. on Transport and Sedimentation of Solid Particles*, (pp. 435–444). Wroclaw,Poland.

Wilson, K. C. (1976). A Unified Physical-based Analysis of Solid-Liquid Pipeline Flow. *Proceedings of the 4th International Conference of Hydraulic Transport of Solids in pipes (Hydrotransport 4), BHRA Fluid Engineering* , (pp. 1-16). Cranfield, U.K.

Wilson, K. C., & Pugh, F. J. (1988). Dispersive-Force Modeling of Turbulent Suspension in Heterogeneous Slurry Flow. *Can. J. Chem. Eng*, 66, 721-727.